INFORMATION TO USERS

This manuscript has been reproduced from the microfilm master. UMI films the text directly from the original or copy submitted. Thus, some thesis and dissertation copies are in typewriter face, while others may be from any type of computer printer.

The quality of this reproduction is dependent upon the quality of the copy submitted. Broken or indistinct print, colored or poor quality illustrations and photographs, print bleedthrough, substandard margins, and improper alignment can adversely affect reproduction.

In the unlikely event that the author did not send UMI a complete manuscript and there are missing pages, these will be noted. Also, if unauthorized copyright material had to be removed, a note will indicate the deletion.

Oversize materials (e.g., maps, drawings, charts) are reproduced by sectioning the original, beginning at the upper left-hand corner and continuing from left to right in equal sections with small overlaps. Each original is also photographed in one exposure and is included in reduced form at the back of the book.

Photographs included in the original manuscript have been reproduced xerographically in this copy. Higher quality 6" x 9" black and white photographic prints are available for any photographs or illustrations appearing in this copy for an additional charge. Contact UMI directly to order.

UMI

A Bell & Howell Information Company
300 North Zeeb Road, Ann Arbor MI 48106-1346 USA
313/761-4700 800/521-0600

SAW HUMIDITY SENSOR AND AN ENVIRONMENTAL ELECTRONIC NOSE SYSTEM

Nehad M. Tashtoush

A Thesis

in

The Department

of

Physics

Presented in Partial Fulfillment of the Requirements
for the Degree of Doctor of Philosophy at
Concordia University
Montreal, Quebec, Canada

October, 1996

ABSTRACT

SAW Humidity Sensor and an Environmental

Electronic Nose System

Nehad Tashtoush, Ph.D.

Concordia University, 1996

A polymer-coated surface-acoustic-wave dual delay line oscillator of 50MHz fundamental frequency has been successfully applied as a humidity sensor. A YZ-cut lithium niobate substrate was used. The polymer (polyXIO) was deposited directly over the substrate or over a metal film on the substrate. A turn-around in the frequency shift and a jump in the attenuation were observed when the polymer was deposited over the substrate directly, and therefore the relative humidity range cannot be covered completely. It appears that depositing the polymer over a metal film eliminates both the turn-around in frequency shift and the jump in the attenuation. Moreover, the curve was smooth and covered the full range of relative humidity, and the change in attenuation was found to be lower than the non-metallized path. The viscoelastic mechanism appears to dominate for the whole range of relative humidity. The sensor was found to be reproducible with a moderate hysteresis effect, of the order of 5%. The sensor appears to have no cross effects from other gases and seems to be highly selective to humidity.

This absence of cross effects makes the device a good candidate for humidity measurements in general and to eliminate humidity effects in electronic nose systems.

Also, an electronic nose system of four Taguchi Gas Sensors (TGS) was built. It appears that each sensor has a separate response pattern to each gas used in the test (methane, propane, ethylene and ethane), and that the relative humidity affects the behavior of the electronic nose system. The feasibility of discriminating between gases in mixture was demonstrated. The effects of the ambient conditions, especially humidity, temperature, and the concentration of oxygen gas inside the chamber, appears to affect the reproducibility of the system. This results in a non-reproducible output of the sensors which makes it difficult to train the neural network program in order to discriminate between gases at a given value of relative humidity and concentration. Using different kinds of sensors which is more stable under ambient conditions might give more precise results in discriminating between gases and could improve the estimation of the concentration in the mixture.

Acknowledgments

It is my pleasure to express my gratitude to all people who helped me in completing the present work.

Special thanks to my supervisors **Dr. David Cheeke**, **Dr. Nelson Eddy** and **Professor Joe Shin** without whose support, encouragement, sound guidance, and advice, my work could have been considerably more difficult.

I would also like to thank **Dr. M. Lawrence** from the Chemistry Department at Concordia University for the great assistance in supplying us with the polymer. Appreciation goes to **Dr. M. Kahrizi**, the supervisor of the solid state devices lab at the Electrical Engineering Department at Concordia University for letting me use their lab at which the SAW devices were prepared. The assistance of **Dr. C. K. Jen** at the Industrial Materials Institute (IMI) at Boucherville is highly acknowledged. Thanks are also due to **Mr. Mostafa Showleh** in the Physics Workshop and the staff at the Science Technical Center. Also, the help I had from **Mr. Jason Burke** and **Mr. Dylan Togane,** undergraduate students in Physics, in solving some programming problems is appreciated.

Finally, great thanks is addressed to **Mu'tah University** in Jordan for their financial supportduring my period of study.

Contents

List of Figures

List of Tables

Chapter 1

Introduction

As a result of tremendous developments in the industrial sector, it has become necessary to efficiently detect specific materials in certain areas either as liquids or vapors. Until recently, the human nose was the most widely-used instrument to predict the existence of either undesirable gases such as aromatic toxic gases, hydrocarbons, and other solvents, or of desirable aromas such as in the food, brewing, distilling and perfume industries. However, this technique was not efficient in all cases, especially when the target, gas or vapors, that needed to be detected were toxic and/or if a quantitative detection was required as in detection of flammable gases.

Therefore, many experimental techniques have been introduced to overcome the various difficulties (detecting materials in vapor or liquid phase) in this important aspect of our daily life. One of these techniques is the utility of the change in electrical conductivity of some materials, when exposed to

certain targets, due to changes in their chemical or physical properties [1-6]. Following the major developments in generating techniques of many types of acoustic waves - either bulk (BAW) or surface (SAW) - in piezoelectric materials, such as quartz and lithium niobate, another technique has been developed. This technique is based on the fact that the properties of the piezoelectric material may be changed due to changes in the ambient conditions and/or changes in a sensitive material overlaid onto the substrate. These changes in properties of the substrate or the overlaid sensitive material affect the properties of any acoustic wave, SAW or BAW, generated on the substrate. The most important properties of the acoustic wave that may be affected are the wave velocity and its amplitude. Since it is easy to measure both the wave velocity and its amplitude using readily available instruments, these measurements have been used as a tool to detect gases, liquids, and certain changes in the physical properties of materials including mechanical properties [7-22].

In order to determine a suitable technique to design and build a sensor which is sensitive to a certain target, the target phase, *i.e.* vapor or liquid, is an important issue. This is due to the fact that some techniques can not be used in liquid even though they have good performance for detecting gases, while others have the advantage of functioning well in liquids with no degradation in performance. The best example to explain these cases is the

surface acoustic wave (SAW) method which can be used to detect targets in the gas phase. But the waves will normally be heavily attenuated because of their high velocities, when generated in a liquid. On the other hand, bulk acoustic waves (BAW) or Lamb waves can be used to build sensors for detecting targets in liquids because of their low operational frequencies; hence low velocities. Moreover, most of the sensors which utilize the change of electrical conductivity as a technique are better at detecting targets in the gas state rather than liquid due to the strong effects of liquids on the electrical properties of the sensitive material.

There are other important factors that should be considered in order to have a sensitive device for a specific target using a certain technique. Some of these factors are:

1) The substrate on which the sensitive material will be overlaid. The various physical parameters belonging to each substrate such as the elasticity constant, the magnitude of the wave velocity in that substrate, the thickness of the substrate, and the dielectric constant of the substrate can affect the output signal. Silicon, piezoelectric materials such as quartz and lithium niobate, and other substrates which are coated with a piezoelectric material are common examples.

2) The sensitive material that must be used to detect the target. This

material must be able to interact in a specific chemical interaction with the target and cause some physical or chemical change in its properties. Moreover, the sensitive material must be resistive to ambient conditions such as water vapor and temperature in order to have a long life-time of the sensor. Moreover, the sensitive material should have a reversible behavior when absorbing the target, gas or liquid, in order to keep using it for a long time. Metal-oxide semiconductor materials such as SnO_2, polymers, and metals such as palladium (Pd) are some example of sensitive materials having the above qualities.

Generally speaking, many types of acoustic waves, such as BAW and Lamb-waves, have been used in sensor applications to detect material in liquids [9,10]. However, SAWs have been widely used in different sensor applications, in particular, in chemical gas applications [11-16,18-20,22]. This is due to their high sensitivity to both physical and chemical properties and the fact that they, the SAWs, can be easily generated on a substrate with a very wide range of frequency using inter-digital transducers (IDTs, which were invented in 1965 by White and Voltmer [23]). Also, SAWs have been used in designing and building sensors to detect changes in physical properties of materials as well as in atmospheric measurements, to determine pressure, temperature, and relative humidity [15,16,24,25].

If the technique to be used is determined and the substrate together with

the sensitive material are chosen, it is possible to build a sensitive sensor for a specific target, physical or chemical. However, since the sensitive material might be sensitive to many different targets, as well as to the main one, in the surrounding area of the sensor, it is very difficult to detect the existence of the main target. This is a major requirement in most applications, in particular applications which involve flammable gases or toxic materials. This means that the *selectivity* of the sensor is not easily achieved. In other words, if the sensitivity of any sensor is difficult to achieve due to difficulty in finding a suitable sensitive coating material, selectivity is rather more difficult due to the cross effects from other vapors interacting with the coating material.

In order to enhance selectivity, another approach has been reported [26,27]. This approach is based on mimicking the human neural system in distinguishing between different kinds of gases. This system utilizes an array of sensors, each sensor of which has a slightly different degree of sensitivity to some kind of targets in the area surrounding the array. Then, using a suitable neural network program one can discriminate between the targets under test. This system is known as *the electronic nose system.*

In this work we will report upon using surface acoustic waves as a technique in building a sensitive and selective sensor for relative humidity. The sensitive material used in this application is a water-resistive polymer. Moreover, we will report upon the feasibility of using an electronic nose system

which utilizes four Taguchi Gas Sensors (TGS) in its array, in addition to a neural network program to analyze the output measurements to detect and discriminate between certain flammable gases, in particular, methane, propane, ethane and ethylene.

In the next two sections a brief history of the *SAW* relative humidity sensors and electronic nose is given.

In the second chapter, a theoretical background of the *SAW* and possible effective mechanisms are given. Also, the operational mechanism of the TGS sensors as well as basic ideas of the electronic nose are reviewed.

The third chapter is devoted to the experimental detail related to the entire project. It involves a description of the *SAW* device, TGS sensors, experimental procedures and thin film preparation.

The fourth and fifth chapters contain the results and discussion for the *SAW* relative humidity sensor and the electronic nose respectively.

The last chapter includes the conclusions and recommendations for future work.

1.1 *SAW* Humidity Sensors

Since humidity is a common factor in the surroundings and the atmosphere of most of the experiments, measuring and controlling it is a very important issue. Therefore, much work has been done to produce a sensitive humidity

sensor. These sensors are based on either the change in the electrical conductivity of a thin dielectric film [1-6] or on the change in the SAW properties such as velocity and attenuation [15,16]. These changes in the film conductivity or SAW velocity and/or attenuation are due to the adsorption of water vapor molecules in the sensitive material of the sensor.

The word humidity itself describes the water vapor mixed with dry air in the atmosphere [28]. Specific humidity, which is defined as the mass of water vapor present in 1 kg of dry air, is used to measure the moisture content of humid air. It is also known as the humidity ratio or absolute humidity [29]. However, another efficient method for measuring humidity in air is relative humidity (RH). It is defined as the ratio of the prevailing partial pressure P_a of water vapor in the air to the water vapor pressure if the air were saturated, P_s, at a given temperature [28-30]. Hence, this can be expressed as:

$$RH = \frac{P_a}{P_s} \tag{1.1}$$

Multiplying $\frac{P_a}{P_s}$ by 100, one obtain the percent relative humidity.

Many different instruments can be used to measure humidity, either directly or indirectly. For example, an efficient indirect way of measuring humidity is by using the sling psychrometer instrument. It consists of two liquid-in-glass thermometers, one with a cotton wick wrapped around the sensing bulb which spins around very quickly after soaking in water; there-

fore, it is referred to as the wet bulb. The wet bulb temperature will be read by the wetted bulb thermometer while the other thermometer reads the dry bulb temperature. Using the temperature difference between the wet bulb and the dry bulb thermometers, one could measure the humidity in air by referring to what is called the psychrometric chart [29,30].

Since the sling psychrometric instrument does not provide a direct and instantaneous measurement of humidity, it cannot be used for expressing humidity in most of our daily applications, nor in industries. Therefore, direct reading instruments, which are called hygrometers [30], were developed. These hygrometers have a sensitive material that changes some of its properties such as density, conductivity, or elasticity constants, due to the interaction (generally adsorption) with humidity. This change in the sensitive material property or properties can be mathematically correlated to the change in humidity, and can be used to give a direct measurement of it after a calibration procedure. It is important at this point to mention that indirect instruments, such as the sling psychrometer, for measuring humidity are usually used to calibrate the direct instruments, *i.e.* the hygrometers [30].

Many materials, such as semiconducting material and polymers, have the potential of being the sensitive part of a SAW humidity sensor. Because of their simplicity in preparation, good functionality and performance at room temperature, in addition to their sensitivity to moisture, polymers are

good candidates. However, their sensitivity to water vapor and the solubility of some kinds of polymers in water are problematic. It has been reported that hydrophilic polymers have the potential of being dissolved in water, and therefore, cannot be a good candidate for a humidity sensor [4,5]. As a result many studies have been done to improve the polymer resistivity to water. These studies came out of four methods to enhance the resistivity of polymers to water [4,5]. One of these methods was copolymerizing the hydrophilic polymer, with a hydrophobic polymer which results in a water resistive co-polymer [2,5].

In this study we report upon a SAW humidity sensor which is based on both the mass loading effect and the elasticity changes due to swelling caused by humidity absorption (*i.e.* changes in the viscoelastic properties of a thin film). The humidity-measuring system chosen for the present study consists of a dual SAW delay line in which the IDTs were deposited on a $YZ-$cut $LiNbO_3$ substrate. One line is used for sensing and the other is for temperature and pressure compensation. The acoustic wave path of the sensing delay line is coated with a thin film, referred to as $polyXIO$, which consists of a random ternary copolymer containing two types of hydrophilic cationic groups and one hydrophobic styrene group which is blended with $poly[(4-vinylpyridine)-costyrene]$ [31].

1.2 The Electronic Nose System

As mentioned earlier, selectivity of solid state devices is one of the main problems due to the cross effects from other gases in the surroundings. In fact, the quality of the device could be determined by its selectivity together with its sensitivity. The selectivity of a device depends on the physical and chemical properties of the molecules surrounding the device together with the sensitive material overlaid over the substrate. If the molecules surrounding the device belong to different kinds of gases having a large difference in their chemical and physical properties, such as their solubility coefficients, molecular size, etc., the selectivity of the device will be high. However, for gases from the same chemical group, having almost the same chemical and physical properties, the cross effects from all gases to the sensor response might be very high and therefore the selectivity will be low. One trivial solution to increase the selectivity is by choosing a good sensitive and selective chemical coating, *i.e.* choosing a chemical coating which is able to interact selectively with the gas under test. However, from a practical point of view, this is really a very difficult task and in most cases cannot be achieved. A good example to explain this problem is the use of the TGS (Taguchi Gas Sensor) sensor in detecting hydrocarbon gases and carbon monoxide (CO). The TGS uses tin dioxide (SnO_2) as a sensitive material and operates at

various high temperatures depending on the application. These sensors are sensitive to all kinds of hydrocarbon gases such as methane, propane and ethane. Some of them are sensitive for CO. However, it is impossible to detect one individual gas from a gas mixture of CO and hydrocarbons using one individual TGS sensor. This is due to the large cross effects contributing from each gas to the sensor output.

Therefore, to overcome the cross effects problem, and therefore increase the selectivity, the electronic nose system has been proposed by Persaud and Dodd [26] in 1982. They reported upon an integrated sensor array to detect specific odours. Two years later, Zarcomb and Stretter [27] reported upon an integrated sensor array to detect flammable gases and toxic vapors. A. Sitar [32], in his Master thesis used the following definition to describe the electronic nose system, "*An electronic nose is an instrument which comprises an array of electronic chemical sensors with partial specificity and an appropriate pattern-recognition system, capable of recognizing simple or complex odours*". This definition shows that the electronic nose system has two basic components, namely the sensor array and the artificial neural network system, or program.

The neural network program, sometimes referred to as the artificial neural network system (ANN), serves the electronic nose system in the same manner as the human neuron system does in collecting data about a certain event

or phenomena. Then processing these data with a large number of internal neurons which finally allow the brain to produce a certain output. The human brain which is the main tool in processing data, is able to think, compare and retrieve data corresponding to the input data at any time. However, the artificial neural network is not able to do so. Therefore, to achieve good results (output) artificial networks must learn to predict an output with respect to a certain input. This learning process can be achieved simply by training the system using very well-defined and known inputs for each individual component in the mixture under certain conditions before testing the system using a mixture of several components. Then, when the system is trained, it will learn to identify a certain pattern as being composed of a specific concentration of each individual component.

After the invention of the electronic nose system, the TGS sensors, which are fabricated by Figaro Inc., were extensively used to construct arrays for electronic nose systems to detect different kinds of gases such as carbon monoxide, hydrogen, methane, H_2S, NO_2 and others [33-36].

In the *SAW* gas sensor applications, the need for devices with high selectivity encouraged some researchers to utilize the electronic nose approach in this field. This was achieved by building an array of *SAW* devices coated with different coatings. In 1986, Ballantine et al. used 12 *SAW* devices with different chemical layers, which were then exposed to 11 vapors, to explore

the feasibility of a *SAW* array in discriminating gases using pattern recognition techniques [37]. Later, many publications utilizing *SAW* sensor arrays with specific pattern-recognition techniques, have been published [38-42].

The concern is now whether only four sensors are able to discriminate between many gases. This investigation was begun by A. Sitar [32], who designed and built the original electronic nose in the Physics Department of Concordia University. In addition, he wrote C and assembly language programs to interface the analogue-to-digital convertor to the computer, and to store the incoming data on hard disk. He also located an artificial neural network (ANN) pattern recognition program, which he used to train the system to recognize individual gases.

Mr. Sitar was able to demonstrate that the system could accurately recognize single gases, but he obtained poor results if the humidity changed in the period between the training and analysis runs. He also continued with some work following his thesis (heretofore unreported): the ANN appeared to be unable to accurately quantify concentrations of component of gases in mixtures involving propane. He assumed the problem was due to saturation of the detectors by propane at higher concentrations which left the other gas undetectable.

The author has taken up the relative humidity problem as a major portion of this thesis. And so the current project is to:

a) Evaluate a new SAW device as a hygrometer, based on the viscoelastic changes in a polymer film.

and

b) To study the humidity effect in an electronic nose system based on four Taguchi sensor array, and then to correct for the humidity effects in order to discriminate between gases. A look-up tables (each table has the response of the four sensors at a specific value of relative humidity), method will be adopted to train the neural network program.

Chapter 2

Theoretical Background

2.1 Surface Acoustic Wave Devices

Piezoelectric materials are unique in their ability to change their physical properties when exposed to external pressure, *i.e.* stress. In fact, exerting an external force on the surface of a piezoelectric material will result in the creation of an electric field across the surfaces. This phenomena is reversible in the sense that if a piezoelectric substrate is exposed to an electric field, a mechanical change, stress, would take place on the substrate. This phenomena appears in such materials due to their chemical structure which can be polarized under external stress. Due to their nature, piezoelectric materials are sensitive to changes in their surroundings. For example, changing the mass in contact with the surface of a piezoelectric material, the ambient temperature in its surroundings, or the pressure can create a change in its mechanical properties and hence, an electric field will be created. The most

well-known and widely-used piezoelectric materials are quartz (SiO_2) and lithium niobate ($LiNbO_3$).

Therefore, piezoelectric materials have the potential for use in physical and chemical sensor applications to detect various parameters such as mass change, temperature, pressure and different kinds of vapors and liquids.

The invention of interdigital transducers ($IDTs$) by White and Voltmer in 1965 [23] makes it possible to create a mechanical change in a piezoelectric material by applying a voltage, as a radio frequency signal (RF), on its surface using the $IDTs$. In fact, a surface acoustic wave (SAW) could be generated on the surface of a piezoelectric material by depositing two metallic $IDTs$ on its surface and connecting them to an RF signal source. One of the $IDTs$ serves as a transmitter while the second serves as a receiver for the SAW. This configuration is referred to as the delay line (DL). Fig.(2.1) shows the configuration that describes the generation of the SAW in a piezoelectric substrate.

$SAWs$ generated on the surface of a piezoelectric substrate, referred to as *Rayleigh waves*, can be used as a tool to detect certain targets, either liquids or gases. This is because of their dependance on the physical properties of the substrate which might be changed due to various interactions between the target and the substrate such as changing temperature or mass density. In the chemical gas applications, a chemical coating material has to be deposited on

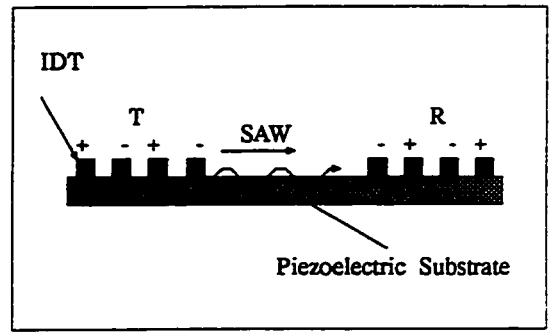

Figure 2.1: Generation of SAW in a piezoelectric substrate using two sets of IDTs, single delay line. The (T) stands for transmitter and the (R) stands for receiver.

the surface of the substrate on the propagation path of the $SAWs$, between the two sets of $IDTs$. Therefore, the detection of a certain gas is based on the ability of the chemical coating material to interact with the target gas, either in a physisorption or a chemisorption interaction. If an interaction takes place, it will create either a physical change in the chemical coating such as its density, or a chemical change such as its electron surface or bulk charge density, *i.e* its charge carriers (if the chemical coating is a conductive one).

$SAWs$ propagating on the surface of a piezoelectric substrate are very sensitive to any change, either chemical or physical, on the substrate and/or the chemical coating overlaid on its surface. In fact, a change in both the SAW velocity and its amplitude, can be used to measure the attenuation,

and this can occur due to a change in the substrate and/or in the chemical coating. In fact, changes in wave amplitude indicate changes in the amount of energy dissipated into the medium contacting the device surface, which therefore signals changes in the physical properties of that medium. The insertion loss reflects the changes in the amplitude of the wave. The insertion loss measures the total energy loss across the device, including transduction losses, propagation losses occurring as the waves travel through the piezoelectric material of the device, and additional losses that occur by dissipation of energy in the fluid or solid medium contacting the device surface. The attenuation coefficient is defined as the rate of change of amplitude per unit distance traveled on the substrate [13]. Therefore, the change in the SAW velocity and the change in attenuation might be used to quantify a change in the chemical coating; and hence, determine the reason for this change, namely the interaction of the target gas in the surrounding area of the substrate. Therefore, both the sensing procedure and the quantification of the gas are achieved.

In the chemical gas sensor applications, where the goal is to detect a specific gas, the sensitivity of the SAW device to many common physical parameters such as temperature, pressure and humidity creates a problem in detecting the target gas. In fact, when a single delay line is used, Δv and $\Delta\alpha$ might be larger due to the change in one of the common ambient

conditions rather than the change due to the target gas itself. Therefore, to overcome this problem, Wohltjen and Dessy [18] introduced another configuration which consists of a dual delay line. In this configuration, one of the delay lines will be used as a sensor, coated with the chemical coating material, while the other will be used as a reference to overcome the effects of the ambient conditions. Many reports have been made using this dual delay line configuration to detect different kinds of gases and chemical vapors [7,8,11-13,15-17,19-21].

Since both the piezoelectric substrate and the chemical coating overlaid on its surface are sensitive to a change in their physical or chemical parameters, any change of these properties might affect the SAW velocity, which is propagating on the surface of the substrate. In fact, the change in the wave velocity (Δv) might be a function of these parameters. Δv can be written in a mathematical relation of these parameters, namely:

$$\Delta v = \frac{\partial v}{\partial m}\Delta m + \frac{\partial v}{\partial c}\Delta c + \frac{\partial v}{\partial \sigma}\Delta \sigma + \frac{\partial v}{\partial \varepsilon}\Delta \varepsilon + \frac{\partial v}{\partial T}\Delta T + \frac{\partial v}{\partial P}\Delta P + ... \quad (2.1)$$

where (Δm) is the change in mass of the substrate and/or the chemical coating, ($\Delta \sigma$) is the change in the conductivity of the chemical coating, (Δc) change in the substrate stiffness, ($\Delta \varepsilon$) the change in the dielectric constant of the substrate and/or the chemical coating, (ΔT) the change in temperature,

and (ΔP) the change in pressure [43,44].

On the other hand, the attenuation of the SAW is found to be affected by changes in the conductivity of the chemical coating and changes in the mechanical properties of the chemical coating, particularly the change in shear modulus G. G can be expressed in a complex form as $G = G' + jG''$. However, it has been reported that the change in mass due to adsorption does not attenuate the SAW [17,20].

In order to build a sensor with high sensitivity for a certain gas, the chemical coating material should be chosen carefully to assure some kind of interaction between the target gas and the chemical coating material. For example, if a conductive material is used as the sensitive part of a sensor, the interaction between the target gas and the conductive material should result in a change of the conductivity of the coating material, a change in its mass, or a change in its mechanical properties to achieve a definite sensitivity. Otherwise it would be very difficult to detect that gas. In fact, it has been found that when a dielectric or conductive thin film is overlaid on a certain piezoelectric substrate, the SAW velocity, propagating on that substrate through the overlaid film, can be affected due to three basic interactions, *i.e.* operational mechanisms, namely:

- The change in the film mass due to the adsorption of gas molecules in the film material. This effect is referred to as the *mass-loading* effect

[8,43].

- The change in the conductivity of the film due to the interaction between the associated electric field with the SAW in the piezoelectric substrate and the charge carriers in the film material. This is brought about by interaction with the target gas molecules. This effect is referred to as the *acoustoelectric* effect [8,43,45,46].

- The change in the mechanical properties of the film material due to the adsorption of gas molecules which might induce a swelling in the film. This swelling induces a change in the shear and bulk modulus of the film and/or induces a change in the film thickness. This effect is referred to as the *viscoelastic* effect [20,21,47-49].

These three effects can contribute to the change in the SAW velocity according to the formula:

$$\frac{\Delta v}{v_o} = -c_m f_o \Delta(m/A) + 4c_c \frac{f_o}{v_o^2} \Delta(hG') - \frac{K^2}{2} \Delta \left[\frac{\sigma_o^2}{\sigma_o^2 + v_o^2 C_o^2} \right] \qquad (2.2)$$

in which c_m and c_c are the coefficients of mass sensitivity and elasticity of the substrate, respectively, (m/A) is the change in mass per unit area, f_o is the fundamental frequency of the SAW device, h is the film thickness, G' is the real part of the shear modulus, K^2 is the electromechanical coupling

coefficient (a measure of the piezoelectric strength of the substrate material), σ_o is the sheet conductivity of the film, $C_o = \varepsilon_p + \varepsilon_a$ is the capacitance per unit length of the SAW substrate material with ε_p and ε_a being permitivities of the substrate and free space respectively, and k is the wave number ($k = 2\pi/\Lambda$; Λ is the acoustic wavelength) [17,20,21,49].

On the other hand, it was found that the attenuation of the SAW might be changed due to a change in one of two factors, which are the conductivity and viscoelasticity changes. However, as mentioned before, the mass-loading effect does not attenuate the SAW velocity. The contribution due to these two effects can be expressed in the following relation [17,20,21,49]:

$$\frac{\Delta\alpha}{k} = 4c_c \frac{f_o}{v_o^2}\Delta(hG'') + \frac{K^2}{2}\Delta\left[\frac{v_o C_o \sigma_o}{\sigma_o^2 + v_o^2 C_o^2}\right]. \tag{2.3}$$

where G'' is the imaginary part of the shear modulus.

It is important to note that if the film is considered to be perfectly elastic (*i.e.* $G'' = 0$) such as in metals, ceramics, and rigid polymers, the change in the shear modulus of the overlaid thin film is very small, and it does not affect the SAW attenuation [20]. Therefore, the shear modulus could be rewritten as

$$G = G' = \mu\frac{\mu + \lambda}{2\mu + \lambda} \tag{2.4}$$

Therefore, Eqn.(2.2) can be rewritten as follows

$$\frac{\Delta v}{v_o} = -c_m f_o \Delta(m/A) + 4c_e \frac{f_o}{v_o^2} \Delta(h) \mu \frac{\mu + \lambda}{2\mu + \lambda} - \frac{K^2}{2} \Delta\left(\frac{\sigma_o^2}{\sigma_o^2 + v_o^2 C_o^2}\right) \quad (2.5)$$

with μ and λ being the Lame constants of the film [8,20,21], while Eqn..(2.3) remains as it is. However, if the film is viscoelastic (*i.e.* $G'' \neq 0$), both Eqn. (2.2) and Eqn. (2.3) apply completely.

Some of the material constants related to Eqns. 2.2 and 2.3 are given in Table (1) [44].

Table (1): Material constants for x-propagating ST-cut quartz and z-propagating Y-cut $LiNbO_3$ substrates.

Substrate	$K^2(\%)$	$c_m(cm^2sg^{-1})$	$c_e(cm^2sg^{-1})$	$v_o(kms^{-1})$	$C_s(pFcm^{-1})$
St-Quartz	0.11	1.28	3.86×10^{-7}	3.16	0.5
$LiNbO_3$	4.80	0.55	1.73×10^{-7}	3.49	4.6

From Eqns. 2.2 and 2.3, one can understand that there are three basic operational mechanisms that may contribute to the sensor response. The existence of any one of them depends on the chemical coating properties. However, one mechanism often dominates the behavior of any sensor. In the next section, a brief description of each operational mechanism will be given.

In practice it is more efficient to measure the frequency shift rather than the changes in the phase velocity. Therefore, a relation which correlates these two parameters has been used [17,20]. That relation is:

$$\frac{\Delta f}{f_o} = \kappa \frac{\Delta v}{v_o} \tag{2.6}$$

where κ is the fraction of the center-to-center distance between input and output transducers affected by the perturbations, (*i.e.* length of the film devided by the length of the device). Therefore, the frequency shift (Δf) will be used to replace change in velocity in all following equations and/or discussion.

2.1.1 Operational Mechanisms

1. Mass-Loading Effect

According to Eqn. (2.2), the mass-loading effect is the simplest mechanism in comparison with other operational mechanisms. In the case of a *SAW* device which is operating with a fundamental frequency f_o, and overlaid by a thin film of a certain material which is sensitive to a specific gas, the measured frequency shift caused by the adsorption of gas molecules in the film material is linearly dependent on the mass change on the surface of the film. This change can be mathematically expressed in the following way:

$$\Delta f = (c_1 + c_2)\Delta(m/A)f_o^2 \tag{2.7}$$

where Δf is the frequency shift, c_1 and c_2 are the material constants for the substrate (for Y cut Z propagation $LiNbO_3$, $c_1 = -3.775 \times 10^{-8} m^2 s/kg$

and $c_2 = -1.73 \times 10^{-8} m^2 s/kg$), and (m/A) is the mass per unit area of the overlaid film (*i.e* ρh, ρ is the film density and h is the film thickness) [8,11,17]. In *BAW* applications, Eqn. (2.6) can be used to determine the thickness of the chemical coating film, which is an important parameter in certain studies. However, in *SAW*, Eqn. (2.6) might be used to estimate the film thickness for specific kind of materials, in particular; soft (rubbery) polymers.

Another important point that should be mentioned concerning mass-loading applications is that the length of the *SAW* delay line does not change the mass-loading effect contribution to the response, since this effect depends only on the mass adsorbed by the overlaid film, *i.e.* by the change in its mass [8].

2. Acoustoelectric Effects

In piezoelectric substrates, the mechanical deformations on the surface of the substrate causes a *SAW* propagating on its surface to create an associated electric field in the substrate. This property of the piezoelectric substrates makes them unique in their ability to detect electrical changes in the surface of the substrate or in the region very close to its surface. In fact, if a *SAW* propagates on a piezoelectric substrate, which is coated with a conductive film, the electric field associated with the *SAW* will interact with the charge

carriers in the film and affect the film conductivity. This interaction causes a change in both the SAW velocity and attenuation. For example, it has been noticed that when a conductive hygroscopic material, such as certain polymers, is used as the sensitive material of a SAW sensor, the sorption of water vapor molecules changes the electrical properties of the film [16]. Therefore, this change in electrical conductivity has been utilized in SAW chemical gas applications [15-17,19,45,46].

From a theoretical point of view, the acoustoelectric effect has been studied in detail [43,45,46,50]. It was found that there is an associated electric field propagating with the SAW propagating on the surface of a specific substrate. This electric field gives the SAW devices a unique property of being sensitive to the electrical change in the film deposited over the substrate or its surroundings.

In the case of using an electrically conductive coating film, an analytical approximate expression to predict the SAW velocity shift and attenuation due to the electrical conductivity change has been derived [43,45,46]. A brief discussion of the methodology used to derive that equation will be considered.

Fig. (2.2) show a typical SAW device which is coated with a conductive film in the x_1x_3 plane. The surface electrical potential φ associated with the SAW propagation in the x_1 direction can be described by:

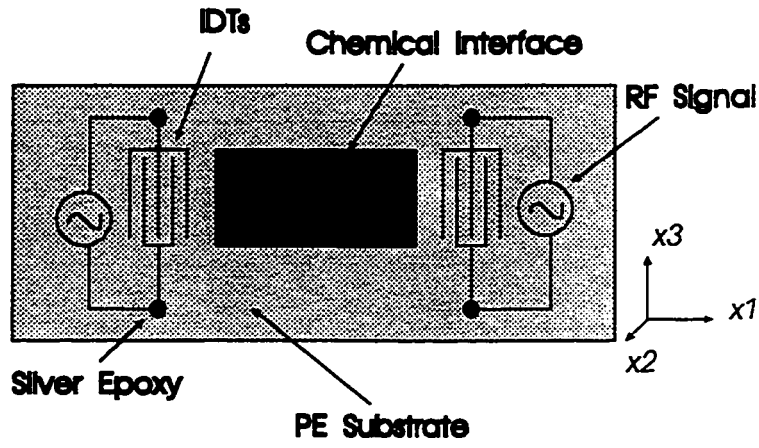

Figure 2.2: SAW Sensor with an overlaid conductive film.

$$\varphi(x_1,t) = \varphi_o(x_1)\exp j(2\pi ft - kx_1) \tag{2.8}$$

where

$$\varphi_o(x_1) = \varphi_o(0)\exp(-\gamma x_1) \tag{2.9}$$

where $\gamma = \alpha + j\beta$ is a complex SAW propagation factor arising from the wave/carrier interaction; and it represents a change in the propagation factor from that of the unperturbed wave [46,50].

The propagation factor γ is a very important parameter for a complete description of the electrical potential $\varphi(x_1)$. Perturbation theory has been used to calculate γ by calculating the power transferred to mobile charges by

the unperturbed potential φ due to small variations in γ [43,45,46,50]. The final result of these analytical studies can be summarized in the following two equations which describe both the change in frequency shift and the change in the attenuation of a SAW propagating on the surface of the substrate due to the change in the film sheet conductivity. These equations are:

$$\frac{\Delta\alpha}{k} = -\frac{K^2}{2}\Delta\left(\frac{v_o C_o \sigma_o}{\sigma_o^2 + v_o^2 C_o^2}\right) \tag{2.10}$$

and

$$\frac{\Delta f}{f_o} = -\frac{K^2}{2}\Delta\left(\frac{\sigma_o^2}{\sigma_o^2 + v_o^2 C_o^2}\right) \tag{2.11}$$

wityh the same parameters defined earlier. It was shown that, for a lithium niobate substrate, the significant changes in frequency shift and attenuation occur only in the range $\frac{v_o C_o}{\sigma_o}$=10^{-2} to 10^2 and the maximum change in the attenuation per wave number ($\frac{\Delta\alpha}{k}$) and the frequency shift ($\frac{\Delta f}{f_o}$) is when $v_o C_o$ = σ_o [45,46,50,51].

The theoretical behavior of this acoustoelectric effect, as found by Eqns. 2.10 and 2.11, is shown in Fig. (2.3).

Many experiments have been done which show that film conductivity changes are the major contributions to the SAW sensor response when an electrical conducting or semiconducting overlay film is used in the SAW propagation path of a delay line[16,45,51,52].

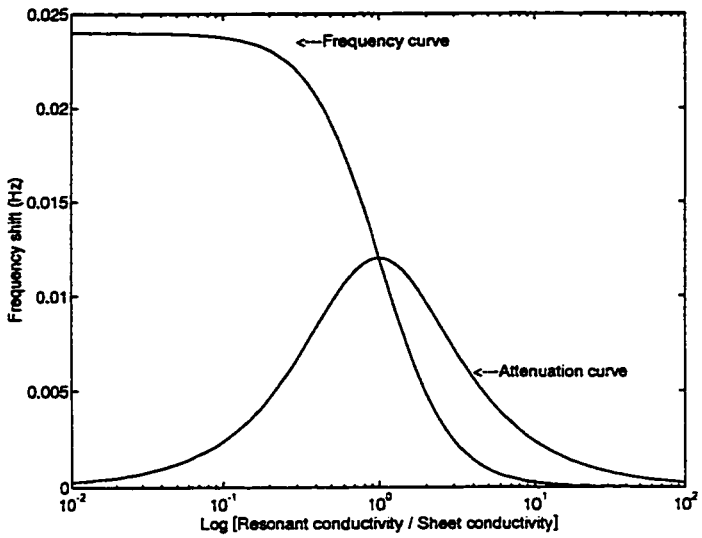

Figure 2.3: Theoretical variation of SAW attenuation and the frequency shift (Δf) as a function of the log of the resonant conductivity to sheet conductivity ratio ($\frac{v_o C_o}{\sigma_o}$) of a conductive thin film.

In order to measure the acoustoelectric effect contribution to a certain gas sensor response, a film of the sensitive material has to be deposited over a metallized path. This means that a thin metal film ($\approx 0.1\mu m$) must be deposited over one line of the dual delay lines of the SAW device (the reference). Then, the polymer thin film has to be deposited uniformly, as much as possible, over both lines (paths). In this configuration, the metal has the effect of shorting out the electric field only on the metallized surface, and hence quenching the acoustoelectric effect on it, while the acoustoelec-

tric effect is still active on the other path (non-metallized). Therefore, the contributions from other possible effects, such as mass-loading, viscoelastic, and/or ambient conditions are cancelled leaving only the acoustoelectric effect to dominate the response (output) of this configuration. [15-17,45,46].

3. Viscoelastic Effects

Fundamentally, a *SAW* propagating on the surface of a piezoelectric substrate causes a mechanical change on its surface. Therefore, when a film of a certain material, such as polymer film, is deposited on the propagation path of the *SAW*, over the substrate surface, the mechanical properties of the film might be changed. In fact, the change in the mechanical properties of the film is a function of deformations caused by the *SAW* in addition to the changes caused by chemical interactions between the film material and some specific gas molecules in its surroundings.

In his book [53], J. D. Ferry described two basic types of deformations that might take place in a certain material, namely: " *From a physical standpoint, the two basic types of deformation are simple shear, which produces a change in shape with no change in volume, and a bulk compression (or its opposite, dilation), which produces a change in volume with no change in shape*". Also, he mentioned that, *"other types of deformation produce a combination of shape and volume changes*". Therefore, in the field of *SAW* gas sensor ap-

plications which utilize a polymer film as their sensitive material, the change in the mechanical properties of the film (shear, bulk or others) can be used as a probe to detect a certain gas. This implies a certain chemical or physical interaction takes place between the gas and the polymer. Also, the SAW device can be used to detect the change in the mechanical properties of any material, particularly polymers. Recently, the utilization of SAW devices in detecting the change in mechanical properties, and their potential in being used in sensor applications has been reported [17,21,49,54]. However, the application of using the change in viscoelastic properties in building a sensor to detect a specific gas or vapor has not been reported.

As mentioned before, the shear modulus and the bulk modulus are the properties that might change in a film due to the change in gas concentration. These two quantities can be written in a complex form, such as;

$$G = G' + jG'' \tag{2.12}$$

and

$$K_b = K_b' + jK_b'' \tag{2.13}$$

In Eqns. (2.13) and (2.14), both the real and the imaginary parts have a physical meaning. The real part of shear modulus is called the storage modulus, and is defined as [53]: "*The stress in phase with the strain in a*

sinusoidal shear deformation divided by the strain; it is a measure of the energy stored and removed per cycle of deformation, when different systems are compared at the same strain amplitude". On the other hand, the imaginary part of the shear modulus is called the loss modulus and is defined as: "*The stress* 90° *out of phase with the strain divided by the strain; it is a measure of the energy dissipated or lost as heat per cycle of deformation, when different systems are compared at the same strain amplitude*". The same definitions are applied to the real and imaginary parts of the bulk modulus, *i.e.* K_b' and K_b'' respectively. According to these definitions, one could understand that when the shear modulus and/or the bulk modulus of a certain polymer film, which serves as the sensitive material of a *SAW* device, is changed due to the *SAW* deformations (which are sinusoidal), attenuation in the *SAW* as well as a change in its velocity would occur. Generally speaking, in a *SAW* device which is coated by a polymer thin film to detect a specific gas, the gas molecules adsorbed by the film might cause a change in the shear and/or bulk modulus. This change can be detected by tracing the change in the *SAW* attenuation and/or the change in its velocity. The attenuation, which is a measure of the change in amplitude, in the *SAW* is expected to increase as the gas concentration increases. This is due to the deformations caused by the gas molecules to the mechanical properties of the film (especially shear and bulk modulus) which results in increasing the energy dissipation of the

SAW, *i.e.* increasing G''. It was found that the magnitude of the attenuation change depends on the film elasticity properties. For solid, rigid elastic polymers the change in attenuation is very small. However, in the case of soft polymers, the G'' value is large enough to cause a large attenuation in the *SAW* velocity [20,21]. The contribution of the change in the mechanical properties was found to be due to the change in the shear modulus, while the contribution of the bulk modulus is relatively small and can be neglected [21]. This contribution can be represented by the second term of Eqn. (2.2) for the change in velocity and the first term in Eqn. (2.3) for the attenuation change. Namely:

$$\frac{\Delta v}{v_o} = 4c_e \frac{f_o}{v_o^2}(\Delta h G') \tag{2.14}$$

and

$$\frac{\Delta \alpha}{k} = 4c_e \frac{f_o}{v_o^2}\Delta(hG'') \tag{2.15}$$

As seen in Eqn.(2.15), the storage moduli G' affects the change in velocity while the loss moduli G'' affects the change in attenuation as seen in Eqn.(2.16). Since these two variables are related to the energy dissipated and stored in the system, a spring system which moves in a viscous medium has been fully described and used to represent the changes between G' and G'' in a film polymer [20,21,49,53,54]. This system is referred to as "*Maxwell*

model [53]".

According to Eqn.(2.14) and Eqn.(2.15), the response due to a change in the viscoelastic properties is expected to be linear for both the attenuation and the change in velocity. However, this is not always the case because the change in both G' and G'' might be non-linear depending on many factors, such as the polymer mechanical properties as well as the gas in surroundings. These properties determine the polymer film behavior (acoustically thin or acoustically thick) related to the gas adsorption and hence the response behavior (linear or non-linear). Moreover, if the film is soft and suffers from a swelling effect due to gas absorption, which will give rise to the mass-loading effect in addition to the viscoelastic effects. The mass-loading effect could be considered as an indirect effect because it might not happen by directly increasing the mass on the film surface. It affects the sensor by changing its thickness, namely increasing the thickness which has a similar effect as of decreasing the mass. Therefore, the resulting effect would be a superposition of the two contributions, which would then display a combination of a straight line and a curve.

Generally, the change in the SAW velocity depends on the elastic properties of the polymer as well as its thickness. In the case of elastic, solid and rigid polymers the change in gas concentration will cause an increase in the storage moduli of the polymer film, the result of which is an increase

in the *SAW* velocity. However, in a soft, inelastic polymer, the loss modulus is larger than the storage modulus. This causes a phase shift in the shear wave which results in decreasing the velocity as the gas concentration increases. Also, the change in velocity (Δv) might increase as gas concentration increases. However, increasing the concentration further will cause an increase in the phase shift of the shear wave propagating on the film surface (normal to the device surface). When this phase shift reaches the value of $\frac{\pi}{2}$, the change in velocity will reverse its sign, *i.e.* Δv will decrease as the gas concentration increases [21]. Therefore, a "turn-around" in the response is expected to take place in the velocity change response as the gas concentration increases. This phenomena can be explained using the other factor that affects the change in velocity behavior, namely the film thickness.

In describing this behavior, Martin et. al. [21] categorized polymer films, according to their thickness, into two regimes, namely " *films that are thin and rigid behave as acoustically thin: the entire film moves synchronously with the substrate surface, resulting in uniform displacement across the film thickness. Films that are thick or soft behave as acoustically thick: the upper film portions lag behind the film/substrate interface, causing nonuniform displacement across the film thickness*". Accordingly, an increase in Δv as the gas concentration increases will take place in the films which are considered to be acoustically thin, and a decrease in Δv as the gas concentration in-

creases will take place in acoustically thick films. This is, as just mentioned, due to the change in the phase shift of the shear wave in the acoustically thick films rather than in the acoustically thin films, which adhere more rigidly to the substrate surface.

Therefore, starting with a polymer film that might behave as acoustically thin (elastic) as the gas concentration increases, at a certain point it might change its behavior to an a acoustically thick (soft). This is presumably caused by the swelling in the film due to gas adsorption which increases the film thickness and changes its mechanical properties, *i.e.* G and K_b. Due to this change in the film behavior, the SAW velocity might change its behavior from increasing to decreasing at that point ("*referred to as the transition point* [21], *or the plasticization point* [53]") and hence what we referred to as "the turn-around" will occur. It is important to mention that after the "turn-around" point, Martin et. al. found that there will be no contribution of the mass-loading effect to the sensor response [21].

Another important point concerning the viscoelastic properties of polymers is the effect of the metallization of the substrate on which the film is deposited. It has been reported that when a thin metal film is deposited between the polymer film and the substrate, the mechanical properties of the polymer film will change. This was explained due to the polymer/metal interface interactions which result in strengthening the rigidity of the film

and increasing its tolerance for higher degrees of mechanical deformations compared with the case in which the polymer is deposited directly over the substrate [55]. In terms of the viscoelastic properties of the polymer film and the film behavior, the film will behave as acoustically thin (rigid and elastic) against higher values of gas concentrations when deposited over a metallized path. However, when deposited directly over the substrate, it will behave as acoustically thin for lower values of gas concentration and then it will change its behavior to acoustically thick (soft or rubbery) which might result in a turn-around in the change in velocity response or a maximum peak in the attenuation as will be shown in our results.

2.2 The Electronic Nose System

As mentioned earlier, the electronic nose is a system (which imitates the human neural system in discriminating among gases and odors) composed of two basic parts, the sensor array and the neural network program. The sensor array feeds the system with data, which is the response (output) of each individual sensor to a specific gas or gases. Then, these data will be analyzed using the neural network program, which generates a certain output pattern that characterizes gas mixtures and/or identifies a certain gas. In fact, each individual sensor of the array produces an output which is slightly different than the others in the array. At a given concentration,

four detectors will output four numbers, which are called a "pattern". This pattern is unique to the specific sensors used, ambient conditions, and the gas or gases sensed. This output pattern (from the sensor array) is used as an input for the neural network program (NNP). The NNP generates its own pattern by analyzing the input data, then uses this unique pattern to discriminate between different kinds of gases according to their responses (this is why it is referred to as the pattern recognition method or technique). It is important, at this point, to point out the fact that the NNP cannot identify a gas or characterize a gas mixture by just analyzing its input data, *i.e.* by feeding it specific input data. In fact, it must be taught to do so. One must train an NNP with known calibration patterns before it can learn to identify components of a mixture quantitatively. Therefore, the NNP is based on two important as well as necessary procedures which are "the training" and "the learning" procedures.

The training process is based on exposing the system (sensor array) to known gases and well-defined gas concentrations. When the output pattern of the sensor array is fed to the NNP, the later will generate its unique pattern for that specific gas. Moreover, when a set of unique patterns for different kinds of gases is generated (or formed), the NNP will use this unique pattern to discriminate (and hence identify) a certain gas (either individual or in a mixture) by comparing its output pattern from the sensor array and

its unique generated pattern from the NNP. This means that the NNP has learned to identify a certain gas in a gas mixture after it was trained. Hence, the learning process can be thought as the ultimate result of the training process of a certain NNP.

From the above discussion, one could realize that the electronic nose system is very similar to the human nose in its ability and methodology in identifying gases and/or vapors. In fact, the electronic nose system was designed and built to imitate the human nose and to replace it in identifying different kind of vapors and odors which might be either toxic or with a concentration too small for the human nose to detect. In their publication [56], J. W. Gardner et. al. have described the similarity between the electronic nose and the human nose (or human neuron system): "*The human nose contains approximately 50 million cells in the olfactory epithelium that act as primary receptors to odorous molecules. There are about 10,000 primary neurons associated with these primary receptors that synaptically link into a single secondary neuron which in turn feeds the olfactory cortex of the brain. This parallel architecture suggests an arrangement that could lead to an analogous instrument capable of mimicking the biological system*". Fig.(2.4) shows the schematic diagram, based on their description, of both the electronic nose and the human nose systems.

The diagram in Fig. (2.4) shows that the sensor array, in the electronic

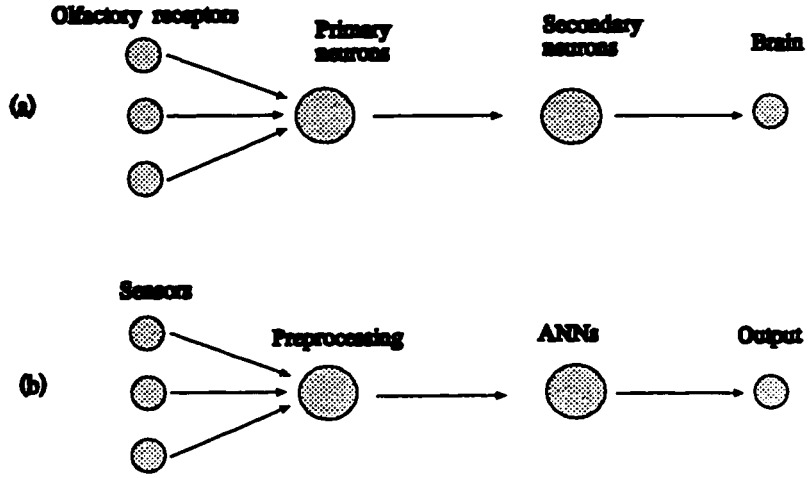

Figure 2.4: Schematic diagram of a human nose system (a) and an electronic nose system (b). [56]

nose system, plays the same role as the olfactory receptors in the human system. The preprocessor part contains two components, namely a data acquisition system composed of an a analog-to digital convertor (used to convert the analog output signal of the sensor array into digital numbers to be fed to the NNP) and a microcomputer system used in collecting the data and saving it for future analysis. In another words, as the secondary neurons do in human neuron system together with the brain, this part (the preprocessor) works on generating the output pattern of the sensor array which will be used as the input data for the NNP either to train it to generate a recognition pattern or to identify the target component (specific gas or odor) of that pattern if it is already trained to do so.

The neural network system is defined as "*an artificial network which mimics a human brain where many neurons are interconnected*". Moreover, in describing its structure, J. W. Gardner said: "*the artificial neural networks consist of parallel interconnected, and usually adaptive, processing elements. The hierarchical organization or architecture of these elements is based upon a physical model of biological neuron systems*" [56]. A physical connection of a typical three-layer neural network is shown in Fig.(2.5).

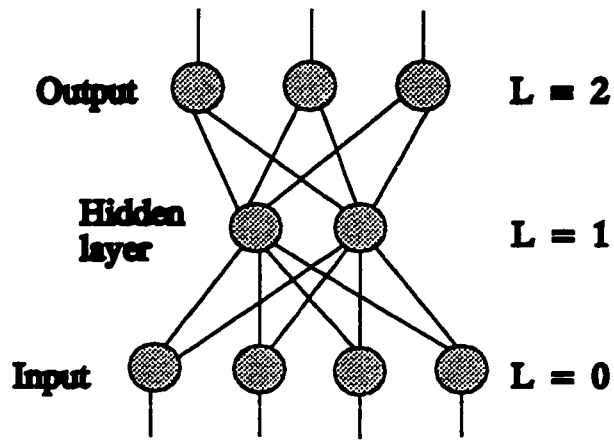

Figure 2.5: Diagrammatic representation of a fully connected three-layer network with 4 inputs (L=0), three outputs (L=2) and 2 hidden layer neurodes (L=1).

This three-layer network consists of three basic processing elements which are, as seen in Fig. (2.5):

- The input layer which is capable of receiving the output data of the

sensor array and to then send it to the next layer for further processing. This layer is fully connected with the next layer.

- The hidden layer, *so called because it is not readily accessible* [56].
- The output layer which gives the results of the processed data.

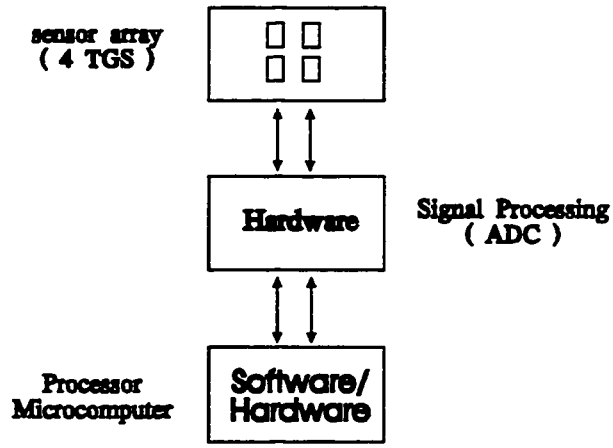

Figure 2.6: Schematic diagram of the electronic nose system used in this study (Concordia Electronic Nose) [32,60].

In this project, the electronic nose experiments will be carried out using an *"Artificial Electronic Nose System [32]"*, which was built and described by Allan Sitar for his M.Sc. project in the Physics Department of Concordia University. Fig. (2.6) shows a schematic diagram of this electronic nose, which is a prototype of the electronic nose system built in the University of

Warwick in Coventry, England (with the exception in the number of sensors in each array) [32,58].

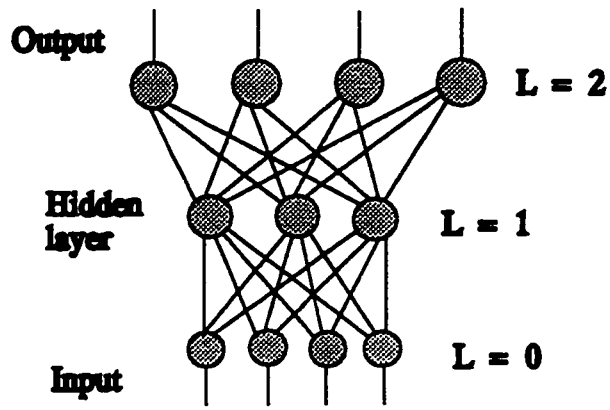

Figure 2.7: Symbolic representation of the three-layer network system used with the Concordia electronic nose, with 4-inputs and 4-outputs [32].

Moreover, a three-layer neural network system which will be used in this project has been described and tested by A. Sitar [32]. This three-layer network is shown in Fig.(2.7).

2.3 TGS Tin Dioxide Sensors

The sensors used in this study are Taguchi Gas Sensors (TGS). They are solid-state sensors mainly composed of sintered tin dioxide (SnO_2) which detects gases through an increase in electrical conductivity when the reducing gases are adsorbed on the sensor's surface [59].

In fact, these sensors operate at high temperatures, ranging between 150

to $500°C$. The high temperature is needed to assure fast and reversible surface interactions with the target gas. Free electrons easily flow through the grain boundaries of the tin dioxide particles, giving the material the property of high conductivity, especially with the absence of oxygen in the surroundings. However, oxygen, which acts as an acceptor, traps free electrons due to its electron affinity. This results in inducing a decrease in the electron density in the surface region, *i.e.* lowering the surface conductivity. When the adsorbed oxygen on the tin dioxide surface is exposed to reducing gases, they react with each other resulting in oxidation of the tin dioxide surface. This reduction reaction increases the electron density in the sensor surface and therefore, increasing its conductivity [59].

The reaction between gases and surface oxygen, and therefore sensor sensitivity, will vary depending on the sensor element's temperature and the activity of sensor material. For example, at low temperatures, it was found that TGS sensors are sensitive to carbon monoxide while they are more sensitive and selective for methane at high temperatures [59]. The manufacturing company, Figaro Engineering Inc., provides different cross sensitivities by selecting the most suitable combinations of sensor temperature and activity of sensor materials.

Chapter 3

Experimental Details

3.1 *SAW* Delay Line

The *SAW* gas microsensor to be used in the present work is shown in Fig. (3.1). It consists of two pairs of aluminum interdigital transducers (*IDTs*). Each one of them has 20 pairs of fingers which have been fabricated on a *YZ* $LiNbO_3$ substrate using photolithographic techniques, forming a dual delay line configuration. One delay line channel is the control or reference channel (path) while the second one, with a film of polyXIO polymer in the propagation path, is the active channel (sensor).

The operating frequency of the sensor is $50MHz$ while the wave length, determined by the *IDT* finger spacing, is $68\mu m$. The *SAW* delay line oscillator consists of a wide band *RF* amplifier having a gain of $\simeq 40dB$, and a feed back network, which is the *SAW* device, connected in a closed loop such that a positive feedback from the output of the amplifier is fed back to its

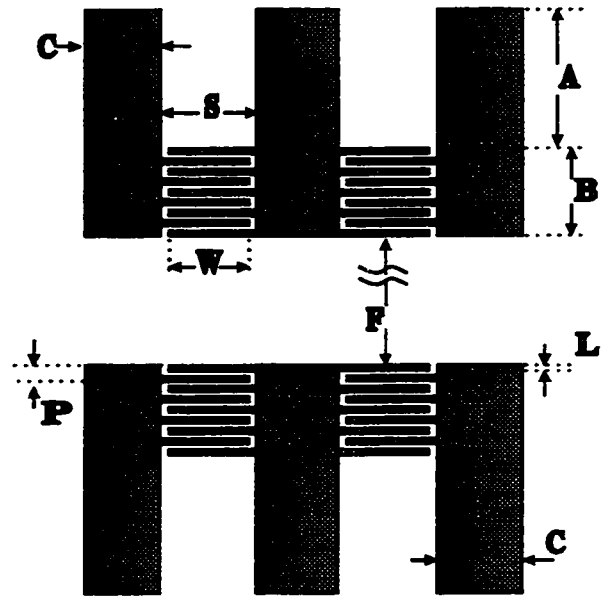

Figure 3.1: Schematic daiagram of a 50 MHz dual delay line. (Designed by: Nehad Tashtoush. # NMT1).

input through the delay line. The oscillation criterion is met when the phase delay is an integral multiple of 2π and the gain exceeds unity. The sensor was characterized using the *H4195A Network/Spectrum Analyzer.*

The frequency response of the device is shown in Fig. (3.2), It shows that the insertion loss of the reference path of the device is -5.3 dB, while the insertion loss of the coated path was about -7.0 dB. The additional insertion loss produced by the hygroscopic film (*polyXIO*) was found to be about 2 dB, and the frequency shift produced by this film was in the range of $150 - 250$ kHz, depending on the thickness, as measured at room

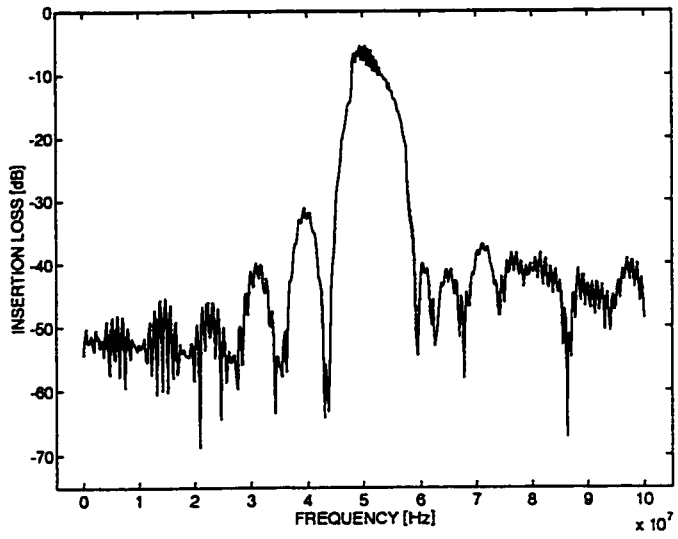

Figure 3.2: SAW device frequency response as measured by the Network/Spectrum Analyzer.

temperature.

3.2 TGS Tin Dioxide Sensors

In our electronic nose system, four commercially available TGS sensors were used to build the sensor array of the electronic nose system. These sensors are of the following models and types:

- sensor #1 is of the model TGS822, and its objectives are to detect organic gases as well as other volatile vapors. Its structure is based on a resin base and housing and considered and referred to as the standard

type.

- sensor #2 is of the model TGS816, and has a sensitivity to a wide range of combustible gases. It has a high sensitivity to methane, propane, and butane. It consists of a ceramic base and a mesh cover to resist to severe environment.

- sensor #3 is of the TGS812, and is sensitive to combustible gases as well as toxic gases. It is specified to be one of the standard type (*i.e.* resin base and housing).

- sensor #4 is TGS813, and has a different sensitivity for methane, propane, and butane It has a resin base and housing.

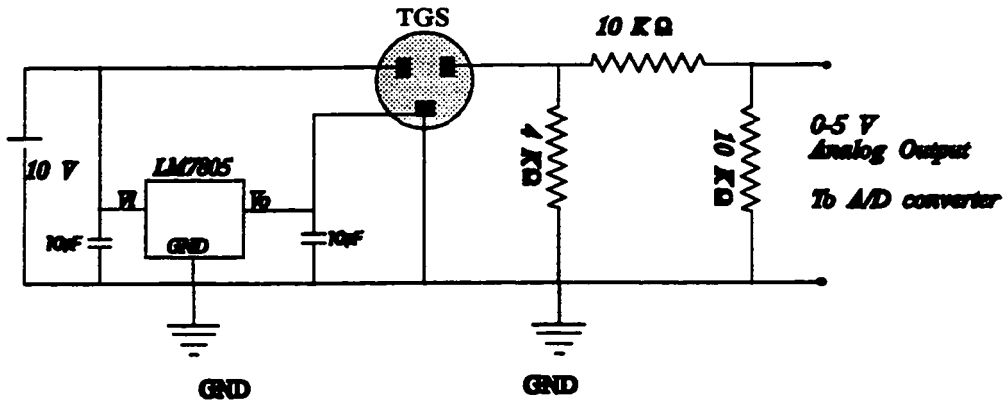

Figure 3.3: The electrical circuit used to drive each TGS sensor in the array. [3]

Fig.(3.3) shows the circuit used to drive each sensor in which a power supply of 10 V is used. Moreover, this circuit supplies a potential difference of about 5 V dc for the integrated heater inside each sensor.

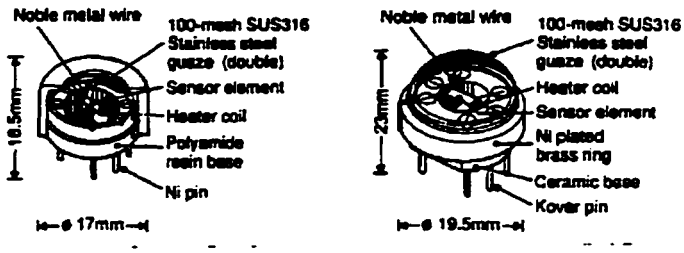

Figure 3.4: The structure of two types of TGS Figaro sensors; (*left*) Standard type, with resin base and package; (*right*) Heat resistant ceramic base with mesh cover. (From Figaro Inc. Reports)

The structure of two types of sensors manufactured by Figaro Inc. is shown in Fig. (3.4). Three sensors were of the standard type (Sensor #1, #3, and #4) and one of them was of the other type (Sensor #2). This kind of sensors can be used to detect combustible gases, CO, H_2 and oxygen in exhaust gases. Any sensor in the array might be sensitive to more than one gas with a slightly different value of response to each gas. For example, sensor #4 (TGS813) is sensitive for both methane and propane as well as other gases and organic vapors. Although the response behavior is similar for each gas, its magnitude is different. Moreover, these sensors are sensitive to humidity

as well as to ambient temperature. These sensors are designed to operate at high temperatures ranging between $150°C$ to about $500°C$. Therefore, these effects should be considered in order to have a good operating sensor or an array of this kind of sensors.

3.3 Experimental Setup

3.3.1 SAW experimental setup

A block diagram of the experimental setup used in this experiment is shown in Fig. (3.5). The sensor was kept inside a box {4} whose walls were made of plexiglass (except the cover which was made from aluminum (Al) to serve as a common ground for the electronic system). $BNCs$ with coaxial cables were used to connect the RF signal from the electronic source to the sensor input and output ports. To mix the gas inside the box within a reasonable time, a small fan was mounted inside the box. A power supply {10} was used to generate power to two electronic circuits. Each one consists of two wide-band frequency amplifiers($NE5205AN$, *Signetics*) with a fixed insertion gain of $20dB$ for each, with a wide band-pass filter {5,6}.

A frequency counter (*Fluke*, $PM6680/B$) {7}was used to measure the output signals from each delay line and is able to give the difference (Δf). The frequency counter was connected to a microcomputer system through a $GPIB$ interface board {8,9}which made it easy, using *Timeview* (software

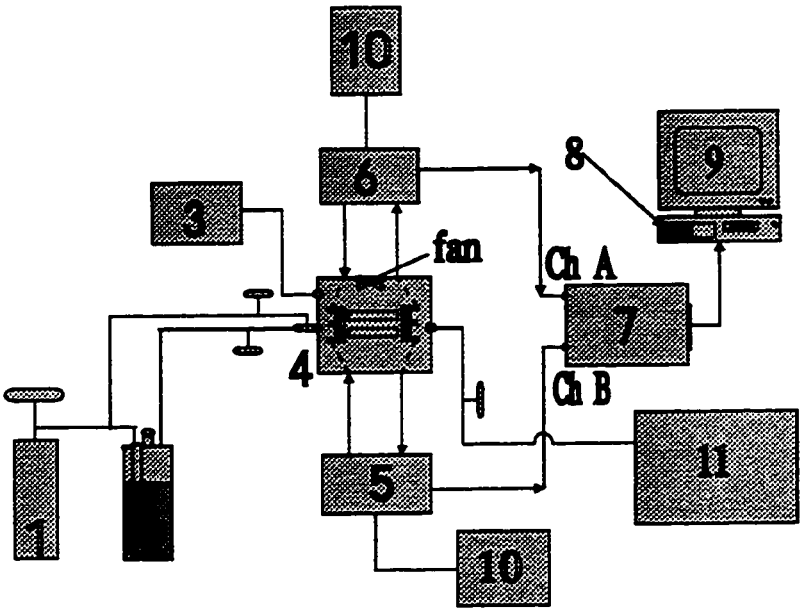

Figure 3.5: Schematic diagram of the experimental setup used for testing the SAW sensor. 1} The nitogen gas tank. 2} The nebulizer. 3} Commercial hygrometer. 4} The chamber in which the SAW device is inserted. 5} and 6} Electronic oscillator circuits. 7} Frequency counter. 8 and 9} GPIB board connected to a microcomputer. 10} Power supplies. 11} Fume hood.

that was supplied with the frequency counter), to collect the data and save it to a text file for future analysis. A small nebulizer {2} *(American Pharmacal Company)*, which is connected to a dry nitrogen gas tank {1} was used to generate humid air to control the relative humidity inside the box. Humidity was decreased by flushing the box with dry nitrogen through another tube line. Relative humidity was measured using a commercial hygrometer *HMP230 Humidity Sensor* (Vaisala){3}.

3.3.2 Electronic Nose Experimental Setup and Procedure

The experimental system used for carrying out the electronic nose experiments consists of a plexiglass chamber in which the four discrete TGS sensors (specified earlier) were mounted. Four holes were made in the chamber sides, two of them were used as a humid and/or dry air inlet and outlet. The third was used to mount a 5 Vdc fan inside the chamber in order to assure gas mixing in a short time, and the fourth was to fix a three-way 12 Vdc solenoid valve (purchased from Cole Palmer products) which is used to inject the gas into the chamber. The system is connected to an ADC (analog-digital convertor) which is connected to a microprocessor to automate and facilitate data collection out of the system.

In this study, four combustible gases (purchased from ProdAir Company) will be used. These gases are methane, propane, ethylene and ethane. Each gas is chemically pure and composed of 99% combustible gas diluted in 1% air. Each gas cylinder was connected to a proper 2-stage gas regulator which is set to a value of 50 psi. Then, the regulator is connected to a Matheson high-accuracy valve flowmeter. The flowmeter has a glass tube with a scale reading printed on it. These readings indicate the flow rate in millimeters and are important to determine the gas concentration in ppm. This is with the help of a special look-up tables supplied with the flowmeter from its company

(Matheson), and a special formula for calculating the gas concentration in ppm was used [32]

$$C_{gas} = \frac{F.t.U}{V} \times 10^6 \ \ ppm \tag{3.1}$$

where, F is the flow rate in millimeters, t is the injection time in seconds, V is the volume of the test chamber (6174 ml in our case), and U is the dilution ratio.

The electronic nose experiments were conducted in a specific procedure which can be described in the following steps:

- Before conducting any experiment, at least 20 minute were given to the system to warm up. This is to allow the sensor to reach its operating temperature and getting stable.

- Using the computer-controlled 3-way valve, the gas is injected into the chamber for 3 seconds. At the end of the third second, the valve will be closed automatically and allow the computer to collect the output of the sensor array using the ADC and the C program written for this purpose.

- The output was collected for about one minute. During this minute 1000 reading were generated from each sensor in the array and the average of the last 500 value is given by the program at the end of each

run. The deviation of each value of the last 500 readings is found to be less than 0.2% of the average value. Each value of these average values (four in each run) will be represented by only one point in the curve of response.

- A commercial hygrometer is used to measure the ambient relative humidity and temperature in each run (*HMP*230 *Humidity Sensor* (Vaisala)).

- At the end of each run, the gas/air outlet was opened to evacuate the chamber from the gas inside it using the vacuum pump connected to that outlet. this process took place fro two minutes to assure a complete evacuation (venting) of the chamber from the gas. This will make clean and ready for the next run.

- After the system is evacuated from the gas, a time of two minutes was given to the system to allow it to stabilize and to equalize. This is because of the pressure changes caused by the vacuum pump.

- The air inlet valve was opened to increase or decrease the relative humidity value to a desired value by injecting humid or dry nitrogen into the chamber.

- The flowmeter reading is changed to another specified value to prepare

for the next run.

- The gas is injected by the solenoid valve and the procedure goes on this way tell the whole range of gas concentration is covered.
- It is recommended to carry on the experiment for another gas in the next day. This is to minimize or eliminate the cross effect of the first gas on the second and to enable the sensors to stabilize due to the changes causes by the first gas.
- All experiments were conducted at room temperature and a specific values of relative humidity ranges between 10% to 60%.

In our experimental system, it was very difficult to maintain a value of relative humidity larger than 60%. This was due to many reasons such as the large time needed to reach that value and then the amount of water vapor generated inside the chamber. This water vapor (which is generated by dry nitrogen gas) will replace the oxygen gas, causing it to decrease in the chamber. Therefore, the oxidation interaction, on which the sensitivity of these sensors are based on will decrease also, resulting in decreasing the sensitivity of the sensors to any reduced gas such as the gases under test. Moreover, the time given to the system after injecting the humid air (to recover the oxygen gas from the surroundings) will let the humidity decrease and hence became unstable for the time of measurement which is about one

minute. Therefore, the best maximum value of relative humidity which we found to be reasonable for our measurements is 60%.

3.4 Thin Film Preparation

The film used, *polyXIO*, consists of a random ternary copolymer containing two types of hydrophilic cationic groups and one hydrophobic styrene group which is blended with *poly[(4-vinylpyridine)-costyrene]*, the structure of both is shown in Fig. (3.6) [31].

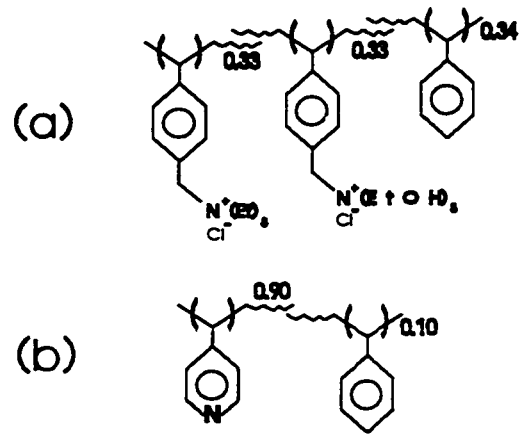

Figure 3.6: Molecular structure of (a) random ternary copolymer, and (b) poly(4-vinylpyridine-copolymer). (M. F. Lawrence et. al. [61])

As described by M. Lawrence, "*the main feature of this type of polymer blend is its spontaneous tendency to segregate into hydrophilic and hydrophobic domains following the casting of films from methanol solution onto a*

substrate" [31]. The hydrophobic domains are essentially composed of the styrene and pyridine moieties of the polymer blend, with their outer walls formed by the hydrophilic quaternized groups. The actual boundaries between these "globule like" domains act as canals for the incorporation of water, and are responsible for the reversible behavior of these films during the absorption/desorption process.

The method of preparation of this polymer was described by Benoit L'Archeveque [60]. To prepare a thin film of this polymer, a drop of bout $100\mu l$ was deposited over the sensor path using a micropipette. In order to have a uniform deposited film, care has been taken to keep the device as flat as possible. This was by laying the substrate on a flat surface to maintain it surface as flat as possible. Then, due to the surface tension and diffusion of the drop, it will expand on the substrate surface in a uniform manner. Nevertheless, our experiments show a non-uniformity in the polyXIO thin film. This has been investigated by casting the polymer over a dual bare path using the micropipette. Moreover, it was noticed that the film color was light brown for very thin films, which were made using about $50\mu l$ of the polymer solution in methanol and depositing it over the desired flat channel. However, to increase the film thickness, more layers were added step by step until we achieved a proper thickness. This was done by adding another $50\mu l$ in each case. The film color started to turn gradually to white (waxy) as the

thickness increased.

Using Eqn.(2.6), with some experimental results we have, such as the frequency shift due to the film deposition over the substrate (which was found to be between 100 to 200 kHz), together with the material constants of the $LiNbO_3$ (k_1& k_2) and the assumption of an average value of $1g/cm^3$ of the polymer density, the thickness of the films was estimated and thought to be in the range of $0.7 - 1.4\mu m$.

Chapter 4

Results of *SAW* Humidity Sensor

Many experiments have been conducted to study the time response, sensitivity, attenuation and reproducibility of the sensor as a function of relative humidity changes. In Fig.(4.1), the experimentally measured variation of frequency shift as a function of time while the relative humidity was changing in the range of $0-67\%$ (adsorption) and $67-0\%$ (desorption) in a period of about 550 s is given for three frequency experiments of a total time of about 1650 s. All measurements were conducted at room temperature on a thin film deposited directly over the substrate. The captured data plotted as Fig. (4.1) shows typical time responses of the sensor to humidity changes inside the chamber. The slope of the adsorption process was calculated and found to be about 0.75 $\%RH/\text{sec}$ during the range of $2\%-66\%$ relative humidity change and was almost the same as for the desorption processes. Moreover,

the response of the SAW sensor appears to be faster than the commercial hygrometer used in the experiment. This was observed by noticing the quick change in the frequency shift as displayed by the frequency counter and the reading displayed by the commercial hygrometer.

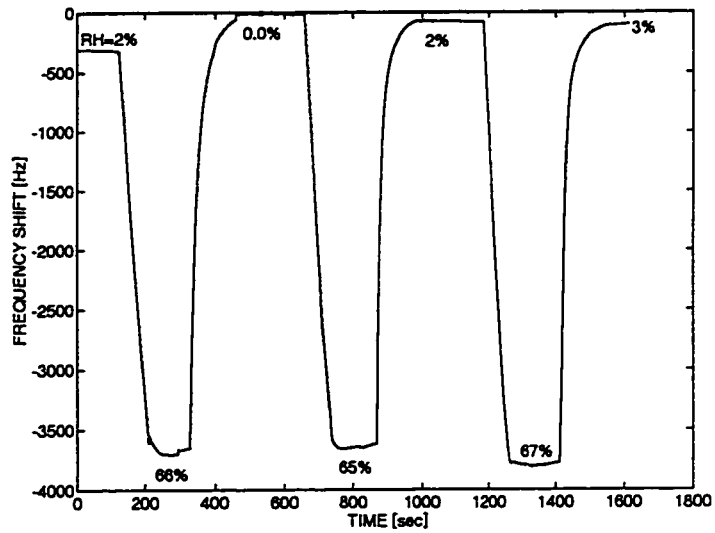

Figure 4.1: Time response of the PolyXIO-SAW humidity sensor during the absorption and desorption process; polyXIO is coated over a bare path.

Two types of experiments have been conducted. First, experiments using what we referred as non-metallized path experiment. We define this as the experiment conducted by using a bare dual path of the *SAW* device. In this experiment the film was deposited directly over the bare path or over both bare paths. Second, experiments utilizing what we refer to as metallized

path. In this type of experiment, a thin metal film was deposited over the substrate. Moreover, the polymer film is deposited either over the metal film or over both metallized and non-metallized paths depending on the purpose of the experiment. The metallization idea was used to sort out the effective mechanisms in the response of the sensor. Therefore, we split the discussion into two parts to clarify the results and eliminate confusion.

4.1 Results of the Non-Metallized *SAW* Device

In order to measure the sensitivity of the sensor, by measuring the frequency shift Δf due to relative humidity changes, an experiment was conducted on the dual SAW delay line having a thin polymer film overlaid directly over the substrate. Fig.(4.2) shows a typical curve of the frequency shift as a function of relative humidity changes. These measurements were performed at $22.5°C$. The response appears to be linear in the humidity range of $0\% - 10\%$. Then it changes to a nonlinear behavior for a higher values of RH. A turn-around at the value of about 82% of RH, for this arbitrary film, was observed. However, as will be shown later, in the experiments performed so far, using different films with different thicknesses, we noticed that the turn-around point depends on the film geometry, especially the thickness. It appears that the thicker the film the lower the value of relative humidity at which the

turn-around takes place.

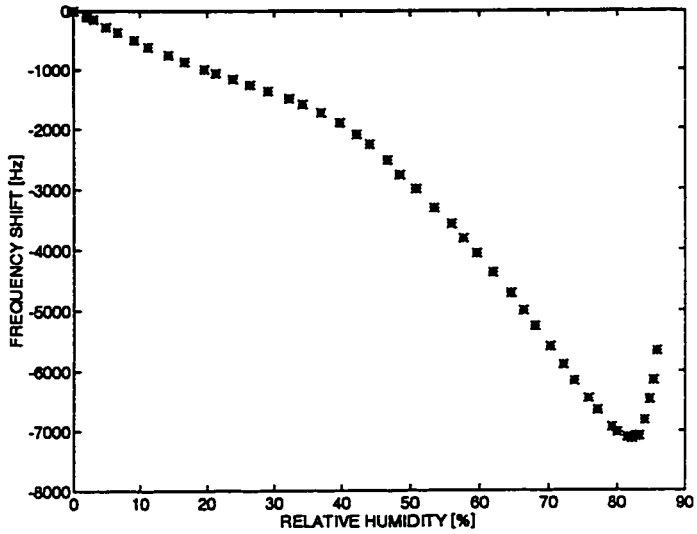

Figure 4.2: Variation of SAW oscillator frequency shift as a function of relative humidity for a polymer-coated SAW device at 22.5°C as measured using a non-metallized device.

The turn-around, *plasticization point*, could be explained as a result of a change in the mechanical properties of the poly-XIO film. At this point, it seems that the polymer changes its behavior from elastic to rubbery which is a result of a change in the phase conditions (of the shear wave) between the upper and the lower surfaces of the film. This change in phase conditions takes place when the change in shear wave phase reaches the value of $\frac{\pi}{2}$.

The same polymer-coated SAW sensor used in the previous experiment

was used to measure the insertion loss (ΔL) as a function of relative humidity changes. The attenuation per wave number was then calculated using the relation [20]:

$$\frac{\Delta\alpha}{k} = \frac{\Delta L}{54.6 N_\lambda} \tag{4.1}$$

where N_λ is the number of waves perturbed by the film ($N_\lambda = 120$ in our case).

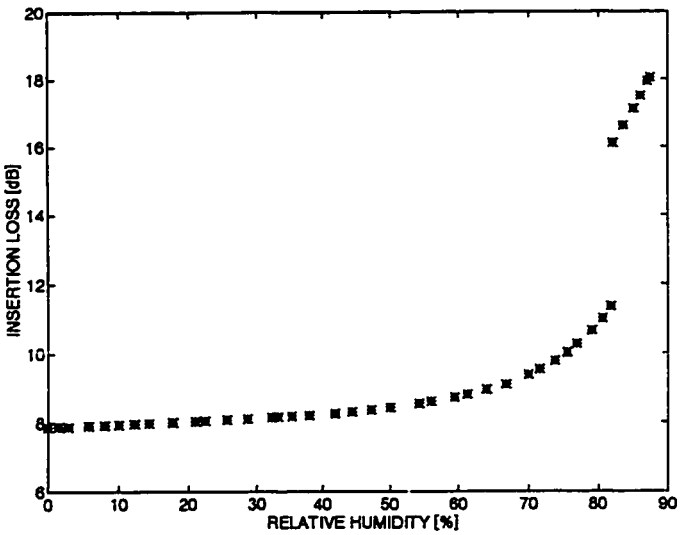

Figure 4.3: Variation of SAW attenuation as a function of relative humidity at 22.5°C for a non-metallized path.

Fig. (4.3) shows the variations in the attenuation as a function of percent relative humidity for the same film used in Fig.(4.2). As indicated in

Fig.(4.3), the change in the attenuation of the SAW seems to be very small in the humidity range of $0\% - 10\%$, after which the attenuation appears to change exponentially. A jump in the insertion loss was observed at a point of about 82% relative humidity, which is the same point at which we observed the turn-around in the frequency shift response. Moreover, the position of the jump appears to change according to the film geometry. Our experiments, in which the film was directly deposited over the substrate, shows that the jump occurred at lower values of relative humidity for thicker films, which is consistent with the results observed in the frequency shift measurements. This jump could be explained as a result of the sudden change in the elastic properties of the polymer film (*i.e.* from glassy regime to rubbery one) which means that the film became lossy.

In order to explain the behavior indicated in both Fig.(4.2) and Fig.(4.3) in more detail and to determine the dominant mechanism in the response behavior shown in Fig.(4.2), an experiment to measure the sheet conductivity (σ_o) of the thin film was made. Fig.(4.4) shows the variation of sheet conductivity, of a polymer thin film deposited over a bare path, as a function of relative humidity. The sheet conductivity of the film appears to be constant up to the value of $60\%RH$, after which the sheet conductivity starts to change exponentially.

Since the attenuation appears to be unchanging in the range of $0\% - 10\%$,

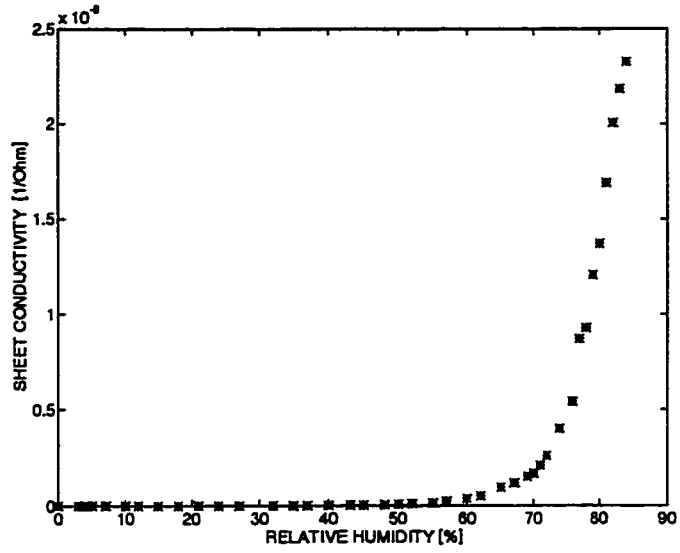

Figure 4.4: Variation of sheet conductivity of the polyXIO film as a function of relative humidity at room temperature.

as indicated in Fig.(4.3), the linear response in Fig.(4.2) for the same range of RH could be explained to be due to the mass-loading effect according to Eqn. (2.2). In the range of $10 - 60\%$ RH, the attenuation is changing exponentially, which indicates, using Eqn.(2.3), that the viscoelastic and/or the acoustoelectric effect(s) might be contributing to the sensor response. However, Fig.(4.4) indicates that there was no change in the sheet conductivity of the thin film, which means that there is no acoustoelectric effect in this region. Therefore, the adsorption response in this range may be thought of as a superposition of mass-loading and viscoelastic effects. For higher values

of relative humidity, it appears that all three mechanisms are contributing to the sensor response.

In order to enhance these results, the captured data of frequency shift (in Fig.(4.2) and attenuation (in Fig.4.3) were plotted against each other, the result of which is shown in Fig.(4.5). The parametric curve shows that the behavior is not, by any means, a semicircle as expected [21,49]. It seems to be constant for very low values of relative humidity (< 5%). Then, attenuation starts to increase gradually as well as the frequency shift. Therefore, one could say that the mass-loading effect appears to dominate at low values of relative humidity, since the attenuation appears to be constant in this range. However, for high values of relative humidity, it seems that all the mechanisms are contributing to the response; since the attenuation is changing in this range of relative humidity. Unfortunately, the information in this curve, Fig.(4.5), and the previous two figures, Fig(4.2-4.4), are not enough to determine the effective mechanism and the dominating one in each range of relative humidity.

4.2 Results of the Metallized *SAW* Device

Since the three mechanisms appear to be contributing to the sensor response, a complete set of experiments was carried out in order to determine the effective and/or dominant mechanism over the whole range of (0 - 100%RH).

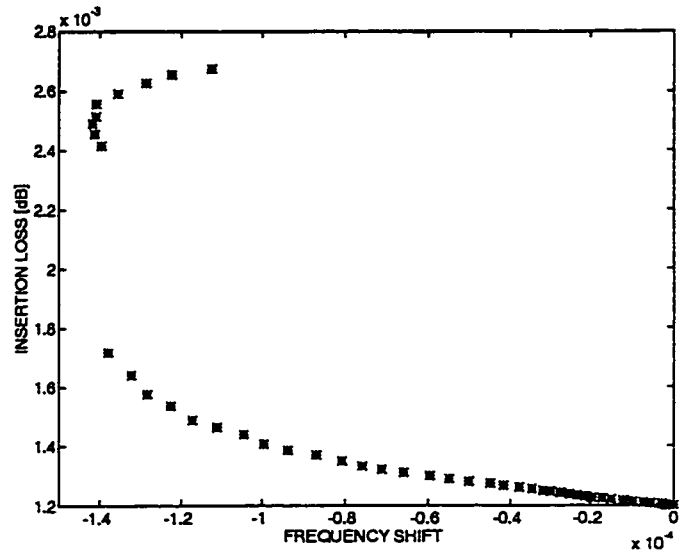

Figure 4.5: Change in attenuation per wave number vs frequency shift as measured with a polyXIO-coated SAW device at room temperature for a non-metallized path.

In these experiments the polymer was overlaid either over a bare path of the substrate or over a metallized one. This comparison is of interest because the metallization shorts out the acoustoelectric effect interaction. The table below shows this set of experiments, in which the symbols N, P, M, and MP stand for

N ≡ Bare Path

P ≡ Only Polymer (Non-metallized) path

M ≡ metallized Path

MP $\equiv$ Polymer over metallized path

Table (2): The set of experiments to be done in order to sort out the effective mechanisms in the sensor behavior.

First path → / *Second path* ↓	N	P	M	MP
N	[N,N]	[N,P]	[N,M]	[N,MP]
P	[P,N]	[P,P]	[P,M]	[P,MP]
M	[M,N]	[M,P]	[M,M]	[M,MP]
MP	[MP,N]	[MP,P]	[MP,M]	[MP,MP]

Fig. (4.6) shows the variation of frequency shift as a function of relative humidity changes for three cases, namely ([N,N], [P,N] and [P,P]). To conduct the first experiment, in which the two paths are bare, the *SAW* device was cleaned using methanol in order to be sure that there will be no trace of polymer over either path. Then the device was returned back to the chamber and the experiment was carried out by increasing the relative humidity up to about 96%. The response appears to be constant for the whole range. The *solid line* in Fig.(4.6) shows the result of this experiment.

The second experiment in this set was to repeat the first experiment done in this study, on which the polymer was deposited over a bare path while the reference is left bare (*i.e.* [P,N] case). Therefore, the device was cleaned again, and a drop of about $50\mu l$ was used to make a thin film over one path of the device. Then the experiment was carried out at room temperature. The

relative humidity was increased gradually up to a maximum value of about 92%. In this experiment we noticed that the turn-around occurred at the value of 89% rather than 82% in the earlier case. The (*) in Fig.(4.6) shows the result of this experiment. Since the value at which the turn-around occurred in this experiment is higher than that observed earlier in Fig.(4.2), it appears that the film geometry (especially thickness) is an important factor. Therefore, in order to check out the effect of thickness, a few other experiments were made. At each one, the thickness was changed (increased) by adding about $50\mu l$ of the polymer solution over the previous film and waiting the proper time in order to carry on a new experiment. Fig.(4.6) is a typical one which shows the result of three different experiments that were made on different films with varying thicknesses.

Fig.(4.6) indicates that the geometry of the film is very important. It appears that the turn-around takes place in each experiment made using a deposited film over one bare path. Also, it took place at higher values of relative humidity for films with smaller thicknesses.

Another experiment was made by depositing the polymer film over both bare paths (*i.e.* [P,P]). In this experiment, every effort was made to ensure that the film was as uniform as possible (as mentioned earlier, by laying the substrate on a flat surface and depositing the drop of the polymer solution onto the center of the area needed to be covered with the polymer). Then the

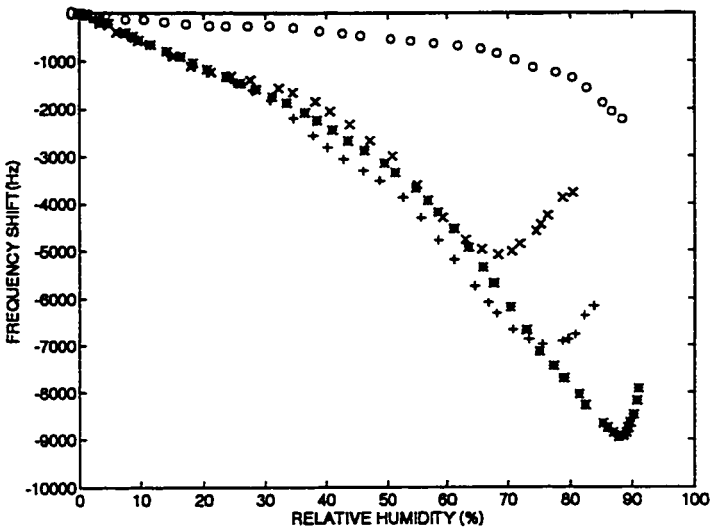

Figure 4.6: Variation of frequency shift as a function of relative humidity for a non-metallized device using different films of arbitrary thicknesses: 1) Films deposited over a bare path while the reference is left bare [P,N]; (*) thickness=h1; (+) thickness=h2>h1, (x) thickness=h3>h2>h1. 2) (o) legend, film cast over the two bare paths of the device [P,P]. $\Delta f = 0$ represents the results of a dual bare device [N,N].

frequency shift was measured as the relative humidity was increased. The result was surprising; the film appears to be non-uniform. The experiment was repeated many times using a new film. The results were essentially identical in all of the experiments. The (o) data points in Fig.(4.6) shows a typical curve of this observation. The magnitude of the frequency shift begins to increase exponentially for values larger than about 30% relative humidity. This indicates that the effective and/or dominant operational mechanisms

are not cancelled in both sides. Therefore, this change in behavior could be explained by the fact that there is more polymer film on one side than the other (*i.e.* the film is non-uniform).

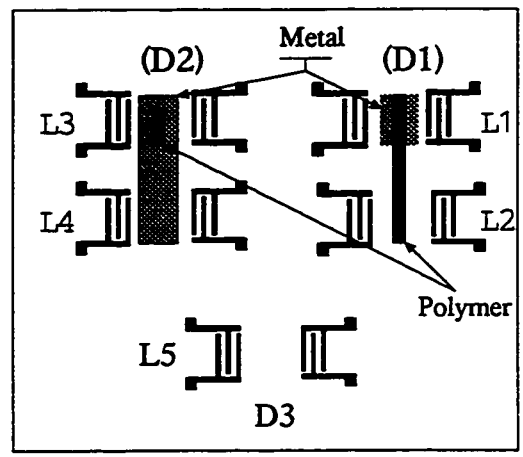

Figure 4.7: Three SAW devices to be used in our experiments; (D1) has a metallized path (L1) with a polymer coated over both (L1,L2); (D2) is metallized over both paths (L3,L4) with polymer over one (L3); and (D3) is a bare path (L5).

In order to study the acoustoelectric effect, two *SAW* devices were built. Fig. (4.7) shows the structure of three SAW devices (D1, D2 and D3) that will be used in the following experiments. On the first device (D1), a thin metal $(Al, 0.3\mu m\ thick)$ was deposited on one of its dual paths (L1), while the second device (D2) has the metal film (of the same thickness) over both paths (L3 and L4). The metal will short out the electric field associated with the *SAW* on that path and hence eliminate the acoustoelectric effect on that

path. Many experiments were performed using the second device (D2), which was metallized over both paths (L3 and L4). Fig. (4.8) shows the variation of frequency shift as a function of relative humidity for a set of experiments conducted using a metallized path. The (o) data points in Fig.(4.8) shows the device response for a free-polymer device (D2 without the polymer, [M,M] case). Then a thin polymer film was deposited over one metallized path while the other metallized path was left bare (D2, [MP,M] case). After taking the frequency shift measurements due to relative humidity changes, the film thickness was increased by adding another layer to the device path. This experiment was repeated many times using various thicknesses to check out the effect of metal and film thickness on the device response. A typical curve for the results is shown in Fig.(4.8), in which the (*), (+) and (x) represent different measurements made on different films with different thicknesses.

Fig.(4.8) shows two important differences between the [MP,M] case and the [P,N] case shown previously in Fig. (4.6). Firstly, the turn-around has been eliminated. Secondly, the entire relative humidity range from 0 to 100% can now be covered with a smooth curve. In order to explain these observations, the attenuation of the metallized *SAW* was measured for every case using the Network Analyzer. Fig.(4.9) shows a typical curve of the insertion loss as a function of relative humidity measured on a film with an arbitrary thickness. This curve reveals another remarkable observation,

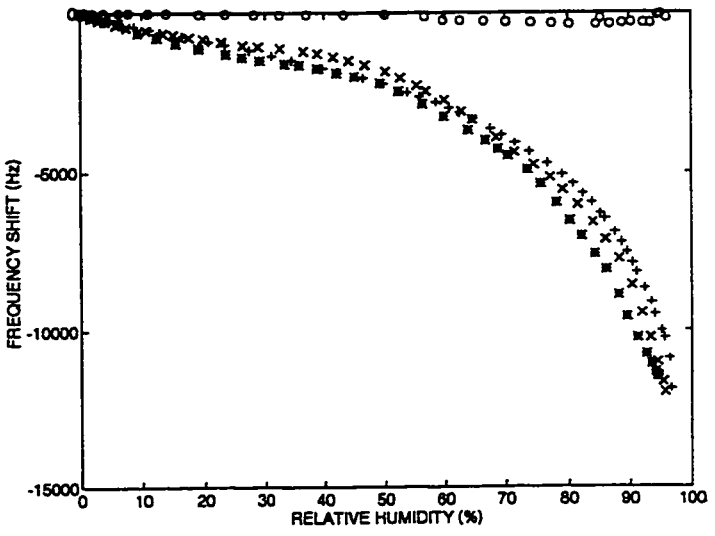

Figure 4.8: Varition of frequency shift as a function of relative humidity for different films of an arbitrary thicknesses using a metallized device: (o) represents the response for a free-polymer metallized device [M,M]; (*), (+) and (x) represent the response for a polymer over a metallized path while the reference is free-polymer and metallized path [MP,M].

namely, the jump which was observed in the case of a non-metallized device (Fig.(4.3)) has also been eliminated.

Comparing the change in the insertion loss for both cases, metallized and non-metallized, one can see that the change is larger for the non-metallized case. This result is very useful to explain the elimination of both the turn-around in the frequency shift and the jump in the insertion loss. However, before trying to speculate on the explanation of these results, we found it

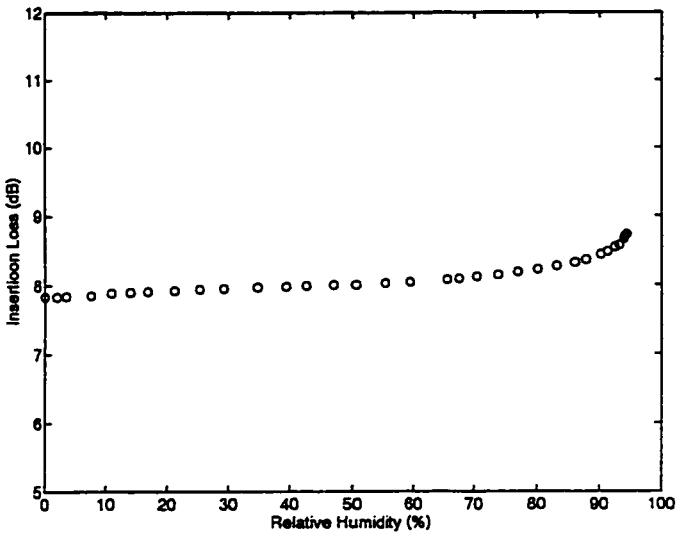

Figure 4.9: Variation of insertion loss as a function of relative humidity for a metallized device at room temperature; [MP] path.

worthwhile to do more experiments, especially an experiment which is able to give some direct information about the acoustoelectric effects on the *SAW*.

For this we used the other device (D1) , in which only one path is metallized (L1) and the polymer is deposited over both paths (L1 and L2, [MP,P] case). Great care was taken to make the film as uniform as possible (as done in the experiments conducted earlier), so that the difference between the two is caused by the metal film. One experiment was conducted using this device. Two other experiments were conducted using another bare device (D3) (under the same ambient conditions) to be used as a reference (L5 in

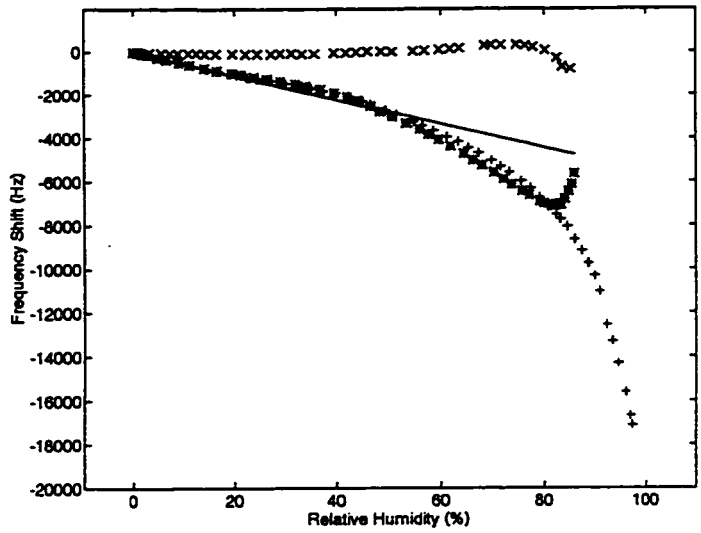

Figure 4.10: Variation of SAW oscillator frequency shift as a function of relative humidity at T=22.5°C for: (*) when polymer deposited over non-metalized path with a bare reference [P,N]; (+) polymer over metalized path with a bare reference [MP,N]; (X) the polymer is coated over both metalized and non-metalized paths (i.e. acoustoelectric effect) [MP,P]; and the solid line is the fitting line of the mass-loading effect data(done by LSM).

Fig.(4.7)). Fig. (4.10) shows the change in frequency shift as a function of relative humidity changes for the three experiments. It is expected to detect the acoustoelectric effect out of the first experiment, *i.e.* [MP,P], due to the metal on the first path (L1), which will short out the electric field on one side. The (X) symbol in Fig.(4.10) shows the result of this experiment. It appears that the behavior is nearly constant up to about 80% relative humidity. After this value of relative humidity the acoustoelectric effect begins

to change the frequency shift. However, in the other experiment, a bare path (L5) was used as a reference and the active path was the metallized one (L1) over which the polymer film was overlaid [MP,N]. This experiment aimed to explore the viscoelastic as well as the mass-loading effects since the polymer is deposited only over a metallized path (L1) where the acoustoelectric effect is eliminated and the other path (L3) is bare. The (+) symbol in Fig.(4.10) shows the result of this experiment. The linear behavior in the low range of relative humidity and the curved behavior at higher values of relative humidity indicate that both the viscoelastic and the mass-loading effects are contributing to the sensor response. Finally, in order to reproduce the results of the non-metallized case, the active path, (L1) on (D1), was switched to the non-metallized one (still coated with the same polymer film, L2 in Fig. (4.7)), while the reference was kept connected to the bare path on the other device (L5), ([P,N] case). The measured values of frequency shift and relative humidity are represented by the (*) on Fig.(4.10).

Also, the attenuation for both metallized (L1) and non-metallized (L2) coated-paths (still the same film) was measured. Fig(4.11) shows the result of these measurements. Fig.(4.10) and Fig.(4.11) show the main differences between metallized and non-metallized substrates. The turn-around in the non-metallized case, the (*) symbol in Fig. (4.10), has been eliminated when a metal is introduced between the polymer and the substrate [metallized (+)].

Also, the jump in the insertion loss in the non-metallized case, the (*) symbol in Fig. (4.11), was eliminated in the case of metallized paths.

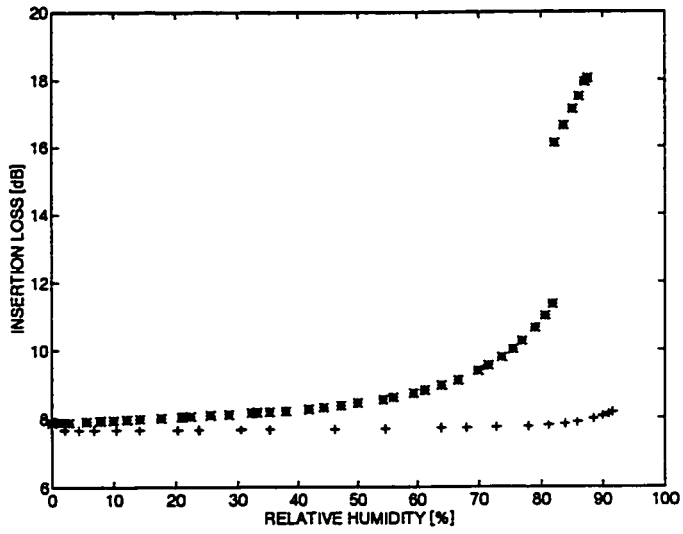

Figure 4.11: Variation of SAW attenuation as a function of relative humidity at 22.5°C for: (*) polymer over non-metalized path; and (+) polymer over metalized path.

Due to the fact that when the polymer is deposited over a metallized path, the polymer/metal (and/or polymer/metal oxide) interaction made the film adhere better to the metal, which in turn binds more tightly to the substrate. This rigidity causes the film to be an elastic film, or acoustically thin. That is, the film is now rigidly adhering to the substrate and is therefore behaving as a rigid (glassy) film. However, without metal, the stiffness coefficient

of the polymer with the substrate is much less due to the absence of the polymer/metal interaction. This results in decreasing the rigidity of the film and therefore decreases its elastic tendency, causing it to enter the rubbery regime, *i.e.* behaving as acoustically thick. This explanation is in agreement with results of G. M. Magomedov et. al., namely: "*the interactions between the polymer and the metal on the metal-polymer interface result in stiffening of the structure of the polymer matrix, which affects the dynamic viscoelastic properties of the polymer. An increase was found in the anisotropy coefficient of the polymer matrix in going from the glassy to the highly elastic state, caused by weakening of the role of the binder in the formation of the properties of the polymer*" [55]. Therefore, referring to the results shown in the previous figures displaying frequency shift and attenuation for all cases, one could say that the polymer film seems to behave as acoustically thin (elastic) when cast over a metallized path while it behaves first as acoustically thin and later (at high RH) as acoustically thick (rubbery) when cast directly over the lithium niobate substrate.

Returning to Fig.(4.10), when the polymer was deposited over both the metallized and non-metallized paths, all effects such as mass loading and viscoelasticity are assumed to be cancelled. Since one path is metallized and other is not, the only expected effect is the acoustoelectric effect. The (x) symbols in Fig.(4.10) show the acoustoelectric effect contribution to the fre-

quency shift response. It appears that the acoustoelectric effect begins to affect the response at higher values of relative humidity (> 80%). At lower values of relative humidity the response appears to be approximately constant with a very small difference between the (*) symbol and the (+) symbol in Fig. (4.10) as a result of individual measurements at different times of the metallized and non-metallized paths. Therefore, referring to Fig. (4.10) and Fig. (4.11), it appears that the mass loading effect dominates in the range of about (0 - 10%RH) whether metallized or non-metallized paths were used. However, since it appears that there is no acoustoelectric effect in the range of (10 - 80%RH), the response might be thought of as a superposition of the mass loading and the viscoelastic effects with the domination of the viscoelastic effect for both metallized and non-metallized paths. For higher values of relative humidity the response is thought to be due to the contribution of the viscoelastic changes and it seems to be the dominant effect, because there is no acoustoelectric effect in the metallized case. Moreover, in the non-metallized case, the attenuation due to the acoustoelectric effect is high enough to block the device from functioning for values larger than 80%, the value after which the acoustoelectric effect appears to have some contribution to the response.

In order to observe the reversibility of the sensor, many measurements were made on different days on the same polymer film. Fig.(4.12) shows a

typical set of curves for the reproducibility behavior. As shown there, the sensor appears to be fairly reproducible for the experiments performed on the non-metallized cases.

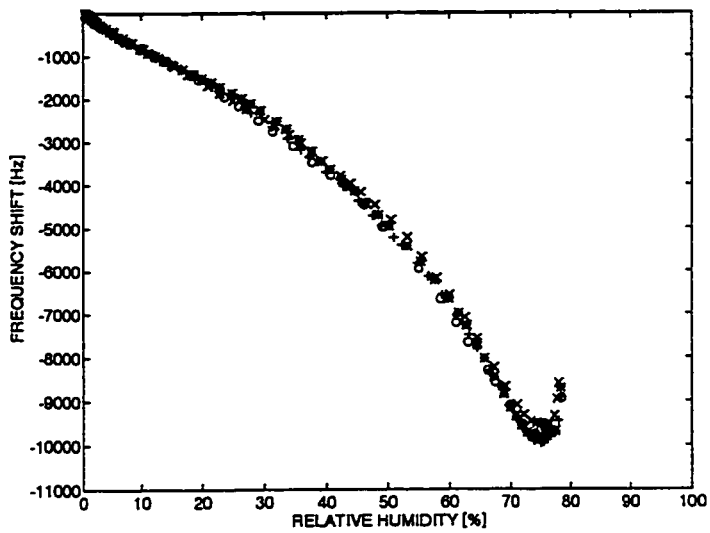

Figure 4.12: Reproducibility of the polyXIO-coated SAW device as measured using a non-metalized path; (o), (+), (*) and (X) represents measurements taken on the same film at different times.

Moreover, the hysteresis effect of most of the polymer-coated devices was studied for both metallized and non-metallized cases. Fig.(4.13) and Fig.(4.14) are typical ones showing the hysteresis effects of the non-metallized polymer-coated *SAW* device and a metallized one, respectively. These two figures show that the sensor appears to be reproducible with a moderate

hysteresis effect of the order of 5%.

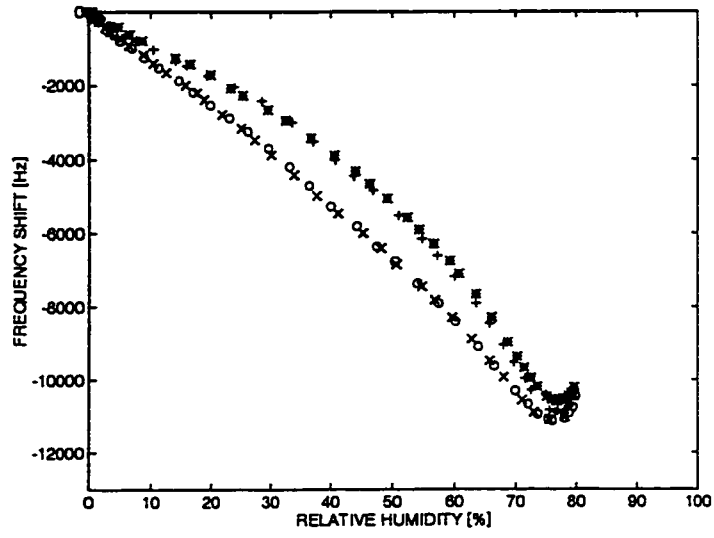

Figure 4.13: Hysteresis effect of the polyXIO-coated SAW device at T=22.5°C, (o) Humidity decreasing; (*) Humidity increasing; (x) Humidity decreasing; and (+) Humidity increasing; measured using non-metalized path.

Finally, the sensitivity of the sensor to many other gases such as carbon monoxide (CO), carbon dioxide (CO_2), oxygen (O_2), methane (CH_4), propane, ethane and ethylene has been studied. It was found to be of the order of a few hertz, which is about 0.05% of the relative humidity sensitivity. Therefore, the sensor appears to be insensitive to all of these gases and appears to be highly selective to humidity. However, since this polymer dissolves in methanol it is expected to have a large response to its vapor and/or

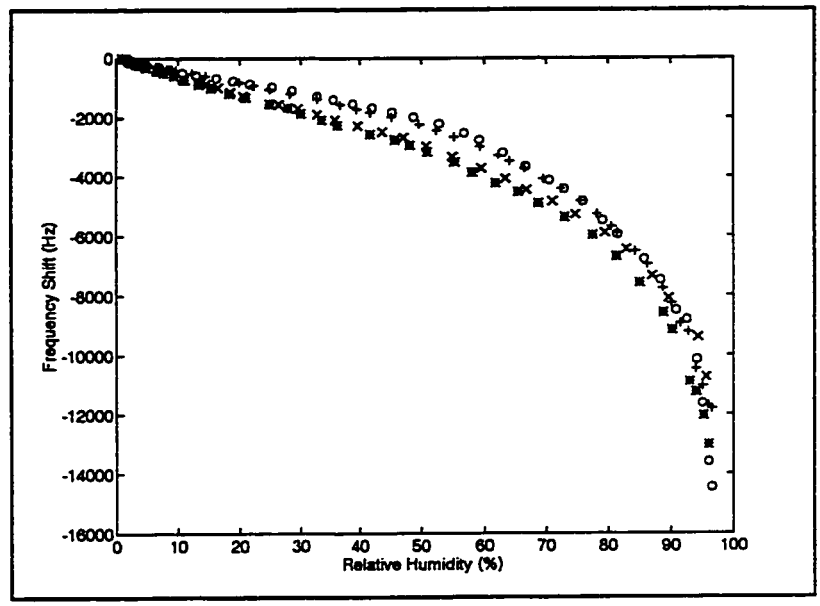

Figure 4.14: Hysteresis effect of the polyXIO-coated SAW device at T=22.5°C, (o) Humidity decreasing; (*) Humidity increasing; (x) Humidity decreasing; and (+) Humidity increasing; measured using metalized path.

other alcohol vapor which have the same chemical properties as methanol such as ethanol [60]. This makes it a good candidate for environmental humidity measurements in general and for eliminating the relative humidity effect in an electronic nose system.

Chapter 5

Results of the Electronic Nose System

In his work, using the same experimental system, A. Sitar made his experiments at random values of relative humidity [32]. This was because that he could not control the relative humidity which was thought to be the reason behind the difficulties he faced in his results. Therefore, the second goal of this project is to control the humidity and study its effects on the electronic nose system. Then, try to correct for its cross effects on the electronic nose system. This will be performed by reproducing A. Sitar results (for sensor array response) by measuring the response of the sensor array for the individual gases used in this study. However, in this study every experiment will be conducted at a specific value of relative humidity rather than random value as Sitar did. Moreover, a complete set of experiments will be conducted for a large range of concentration as well as many different values of rela-

tive humidity. The result of each experiment (the sensor array response as a function of gas concentration at a specific value of relative humidity) will be a part of large number of tables that were conducted at other values of relative humidity. These tables will be used later as a training data set for the neural network program.

5.1 Array Response for Individual Gases

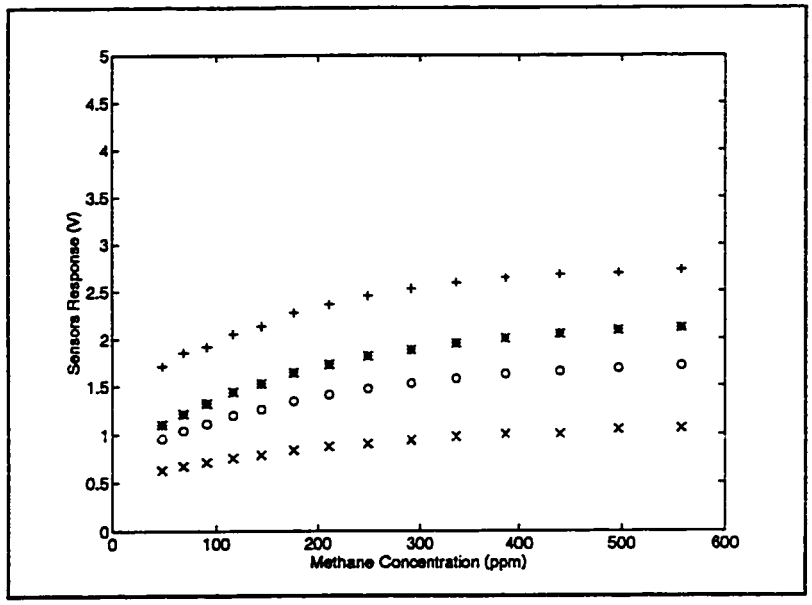

Figure 5.1: Sensors response as a function of methane gas concentration; the legends (o), (*), (x), and (+) represent Sensor #1, Sensor #2; Sensor #3 and Sensor #4 respectively. (At $T = 22^{o}$ and $RH = 20\%$)

Many experiments have been conducted to measure the response of each individual sensor in the array to each individual gas to be tested. This was

achieved by exposing the sensor array to a certain gas in each experiment. All experiments, in this part of the study, were conducted at room temperature and a value of 20% relative humidity with a gas concentration ranges between 50 ppm to 600 ppm. Fig.(5.1) shows the behavior of the 4 sensors of the array as a function of methane gas concentration.

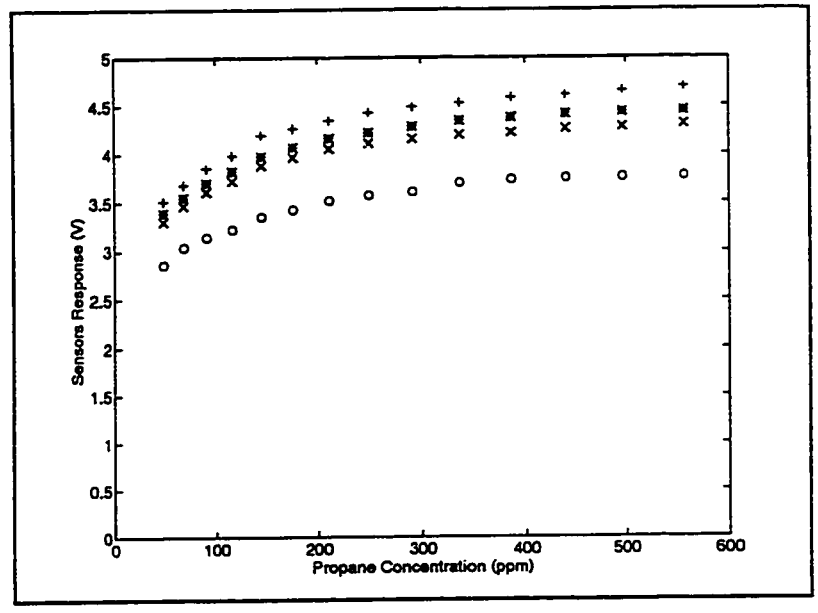

Figure 5.2: Sensors response as a function of propane gas concentration; the legends (o), (*), (x), and (+) represent Sensor #1, Sensor #2; Sensor #3 and Sensor #4 respectively. (At $T = 22^o$ and $RH = 20\%$)

As seen in Fig. (5.1), methane affect the behavior of each sensor almost in the same way, exponentially, but different magnitudes. The sensors order in response is: fourth, second, first, and third respectively, with the fourth hav-

ing the maximum response. In these data, each point is the average of about 500 readings taking during a period of about one minute. The the deviation in this value is very small and found be less than 0.25% ($\mp 0.01V$ about the average value). As Fig.(5.1) shows, the difference between responses of the sensors is in the range of about 1.1 - 1.7 volts over the range of concentration covered. Moreover, the increase in response is large for low concentrations (less than 200 ppm), while it is small for higher values of concentration. The sensors seem to saturate for values higher than about 400 ppm, except the third one which appears to saturate about the value of 200 ppm. This behavior shows what we will referred to as the pattern response of the array for methane gas.

Fig.(5.2) shows response pattern of propane gas. The pattern behavior appears to be the same as that formed by methane gas. However there are few exceptions, first, the propane pattern is located at higher values of response (voltage). Secondly, the order of the sensors is changed in the propane pattern. Finally, the second, third, and fourth sensors appear to have a similar behavior with a small difference in the output voltage, especially at low concentrations. While the response of the first sensor is the lowest and is separated from others by about 0.6 volts over the whole range of concentration. The maximum value of the output voltage was about 4.8 V as measured at room temperature and 20% of relative humidity, while it

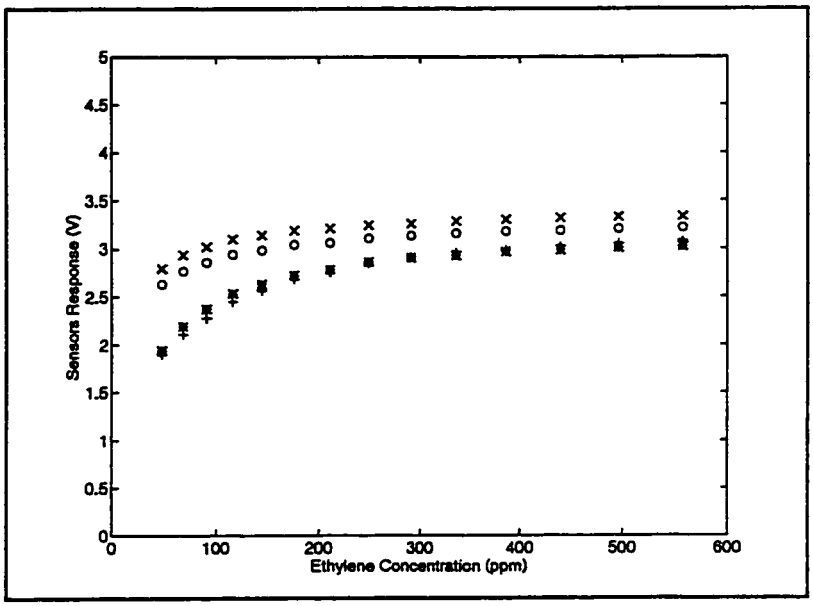

Figure 5.3: Sensors response as a function of ethylene gas concentration; the legends (o), (*), (x), and (+) represent Sensor #1, Sensor #2; Sensor #3 and Sensor #4 respectively. (At $T = 22^o$ and $RH = 20\%$)

was about 2.5 V in the methane pattern. Moreover, propane gas seems to saturate the sensors at a value of about 400 ppm.

Fig.(5.3) shows the pattern generated by ethylene. It appears that ethylene saturates both the first and the third sensors at values of concentrations higher than about 200 ppm, and the other two sensors at values higher than about 400 ppm. Moreover, the first and the third sensors responses are very close together. At the same time, their response is separated and located upper the other two sensors responses which are almost overlapped.

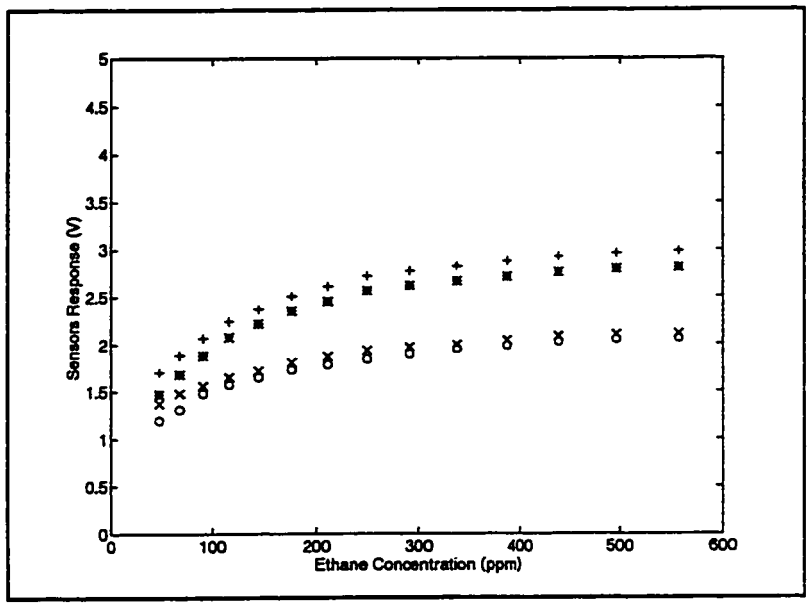

Figure 5.4: Sensors response as a function of ethane gas concentration; the legends (o), (*), (x), and (+) represent Sensor #1, Sensor #2; Sensor #3 and Sensor #4 respectively. (At $T = 22^o$ and $RH = 20\%$)

Finally, the array response to ethane gas is shown in Fig.(5.4). It appears that it is similar to propane (Fig. (5.2)) gas in the order of sensor responses. However, the response of all the sensors appears to begin spliting into two groups as the ethane concentration increases. The fourth and the second sensors form the first upper group, while the third and the first form the other. The ethane appears to saturate the first group at values of concentrations higher than about 500 ppm. While the second group appears to saturate at the values higher than about 300 ppm.

The above discussion shows that the sensors show a unique pattern for each individual gas under test. This is a basic requirement for an array of sensors to be utilized in an electronic nose system. However, there might be some problems such as the saturation of the sensors at low values of concentration (about 250-350 ppm). This will make it difficult to have a wide range of gas mixture concentration for the electronic nose study. Moreover, the high sensitivity of the sensors of the array to propane and ethylene will make it very difficult to have a mixture of both. This can be explained by referring to Fig.(5.2) and Fig. (5.3), two sensors (first and third) will saturate for low concentrations of ethylene (less than 200 ppm). Therefore, adding propane gas to the system will not affect these two sensors and will cause the saturation of the other two. The final result of such an experiment will not be so precise in describing the response or behavior of the array. Also, the relative humidity effect is a major concern since increasing relative humidity will increase the sensor response. This will cause the sensor to saturate at lower values of gas concentration as will be shown in the results of the next section.

5.2 Humidity Effects

In order to sort out the effect of relative humility on the array response, many experiments have been conducted. In each experiment, the controlled

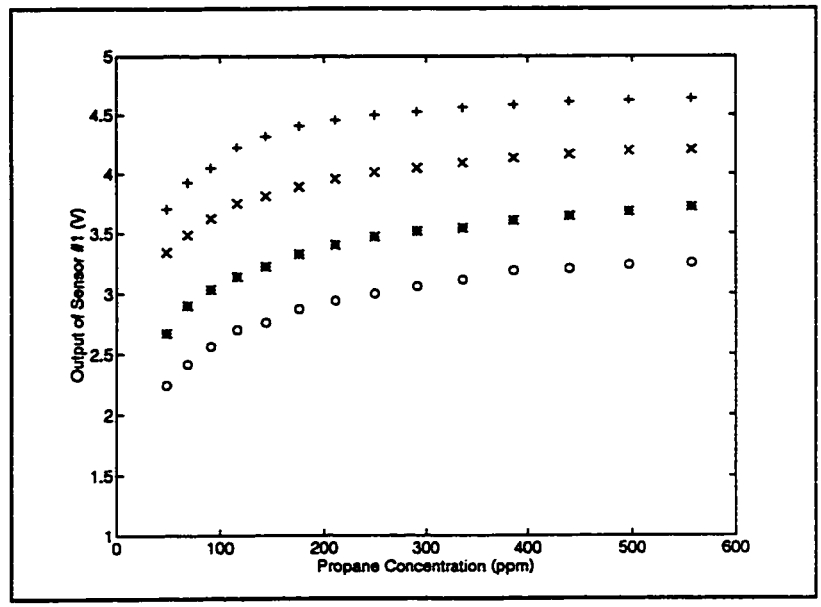

Figure 5.5: The output of sensor #1 (TGS822) as a function of propane concentration at room temperature and different values of relative humidity, namely; (o) 10%, (*) 20%, (x) 40% and (+) 60%.

relative humidity was maintained at a specific value while the concentration of a certain gas is changing to generate a certain pattern. The relative humidity was changed in the range of $0 - 60\%$, with an increment of 10% for each experiment. These complete set of experiments were done for each gas separately in the same manner. It is important to mention that the results of these experiments will be used later as look-up tables for the training process of the neural network program.

Fig.(5.5) is a typical curve which shows the effect of relative humidity on the response of the first sensor in the array as the propane gas concentration

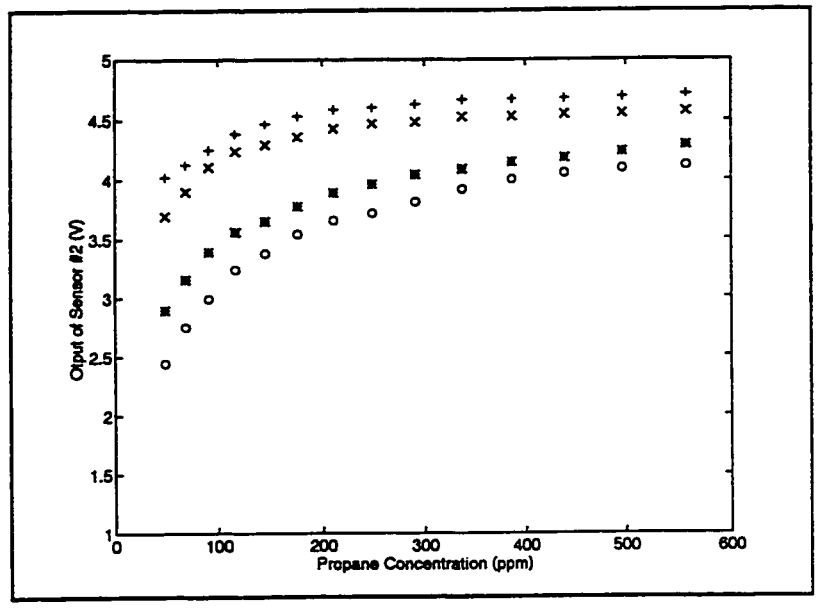

Figure 5.6: The output of sensor #2 (TGS816) as a function of propane concentration at room temperature and different values of relative humidity, namely; (o) 10%, (*) 20%, (x) 40% and (+) 60%.

was changing in the range of $50 - 600$ *ppm*. As shown in the figure, the response of the first sensor is so affected by relative humidity, such that the output voltage difference was about 1.5 V when the relative humidity was changed in the range of 20% to 60% throughout the whole range of gas concentration. Moreover, it appears that the sensor saturates at lower values of gas concentration at higher values of relative humidity.

Fig.(5.6) shows the effect of relative humidity on the response of the second sensor in the array as a function of propane gas concentration. It appears

that at lower values of gas concentration, less than 300 ppm, humidity affects the response more than at higher concentrations. Also, as in the first sensor, the sensor seems to saturate at lower values of gas concentration at higher values of relative humidity.

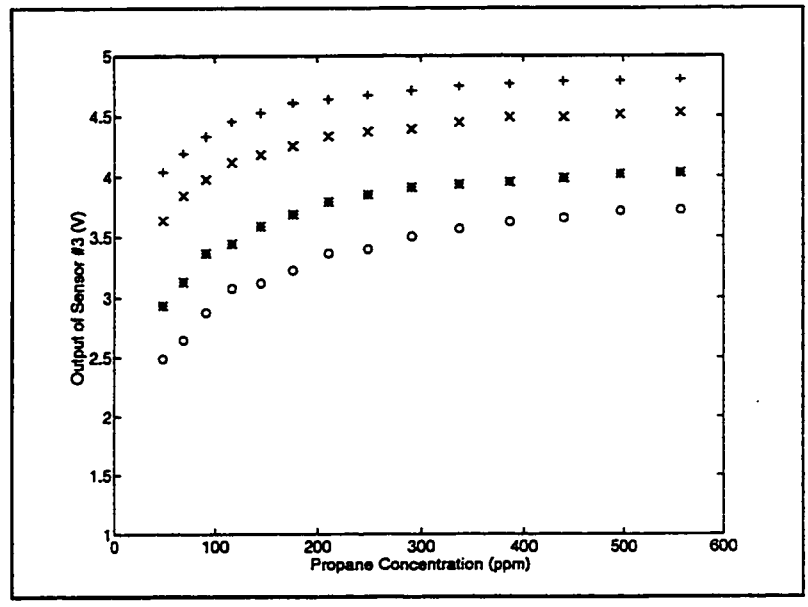

Figure 5.7: The output of sensor #3 (TGS812) as a function of propane concentration at room temperature and different values of relative humidity, namely; (o) 10%, (*) 20%, (x) 40% and (+) 60%.

The average output voltage difference (between the highest and lowest values of relative humidity) at low concentrations of propane was about 2 V, while at high concentrations it was about 1 V. This might be explained by the fact that the sensitivity of this sensor (the second) is larger than that of

the first one, therefore, it saturates at low values after which neither the gas nor the humidity have a large effect.

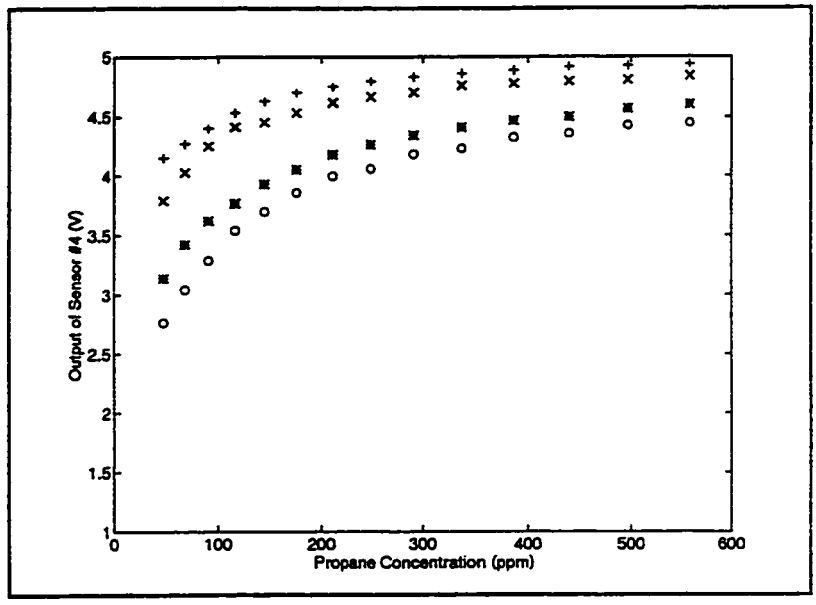

Figure 5.8: The output of sensor #4 (TGS813) as a function of propane concentration at room temperature and different values of relative humidity, namely; (o) 10%, (*) 20%, (x) 40% and (+) 60%.

The behavior of the other two sensors (the third and the fourth) is shown in Fig.(5.7) and Fig.(5.8) respectively. As Fig.(5.7) indicates, the humidity affects the third sensor in almost the same manner as the first one, except that the output voltage difference over the range 20 -60% relative humidity seems to decrease at high values of gas concentrations, *i.e.* larger than 400 ppm. Moreover, this difference in output voltage is larger than that of the second

sensor. Also, the effect of relative humidity on the third sensor saturation behavior is indicated on this figure.

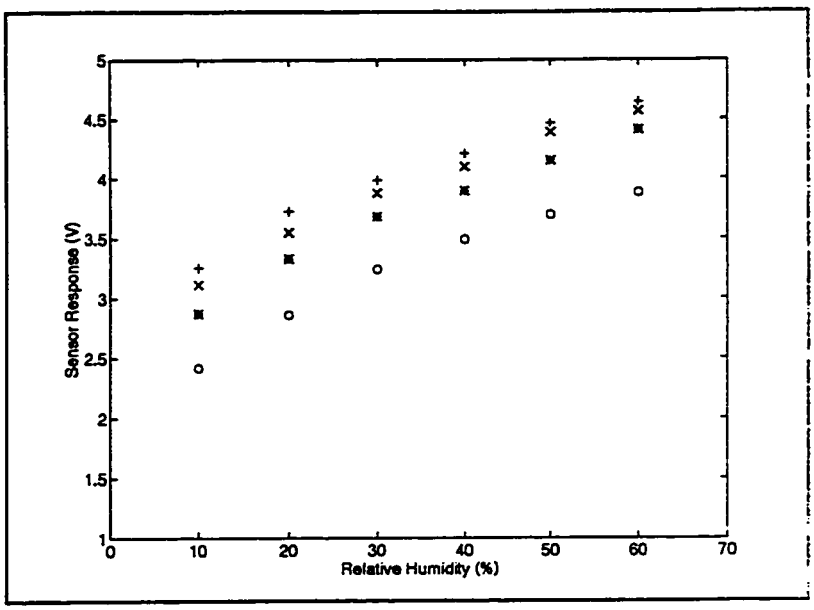

Figure 5.9: Sensor #1 (TGS822) response as a function of relative humidity at different values of propane concentration; (o) 68.5 ppm, (*) 176 ppm, (x) 336 ppm and (+) 557 ppm.

The fourth sensor behavior seems to be the same as the second one, in which the humidity effect is larger at lower values of gas concentration and small for high values of gas concentration. Moreover, as in the previous sensors, the increase in relative humidity saturates the response of this sensor at lower values of gas concentrations.

The last four experiments have been repeated using the other combustible

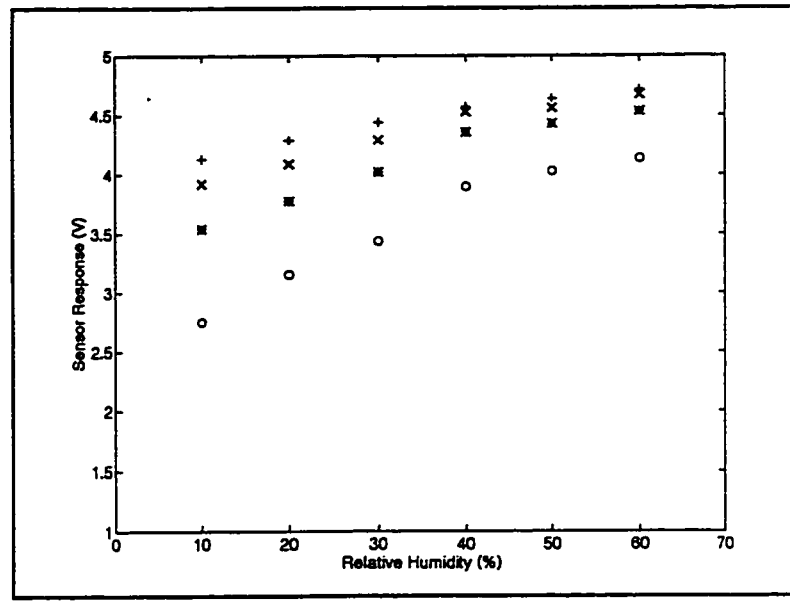

Figure 5.10: Sensor #2 (TGS816) response as a function of relative humidity at different values of propane concentration; (o) 68.5 ppm, (*) 176 ppm, (x) 336 ppm and (+) 557 ppm.

gases we have, namely, ethane, methane and ethylene. The same results have been observed for the humidity effect on each individual sensor of the array.

In order to check out the sensors response as a function of relative humility, the results of previous experiments were used to obtain this relation. Fig.(5.9-5.12) show the effect of relative humility for each individual sensor in the array, at different values of gas concentration. The Figures reveal a remarkable observation, which is that the sensors response behavior due to relative humidity changes seems to be the same as any other tested gas used

in this study.

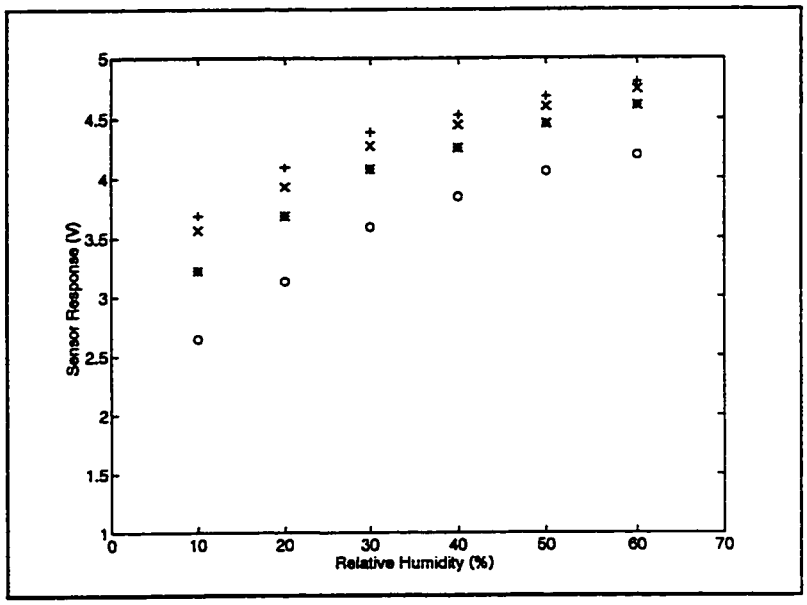

Figure 5.11: Sensor #3 (TGS812) response as a function of relative humidity at different values of propane concentration; (o) 68.5 ppm, (*) 176 ppm, (x) 336 ppm and (+) 557 ppm.

For example, the figures 5.9-5.12 show that increasing relative humidity seems to give an increase in the output voltage which still appears exponential, although the rate of increase is less than that of fuel gases.

In particular, sensors #2 and #4 show a definite trend toward saturation at the top of the humidity range, with sensor #3 showing a weaker effect. However, the first sensor appears to have some peculiarity in that saturation does not occur in this range of relative humidity but seems to be at higher

values.

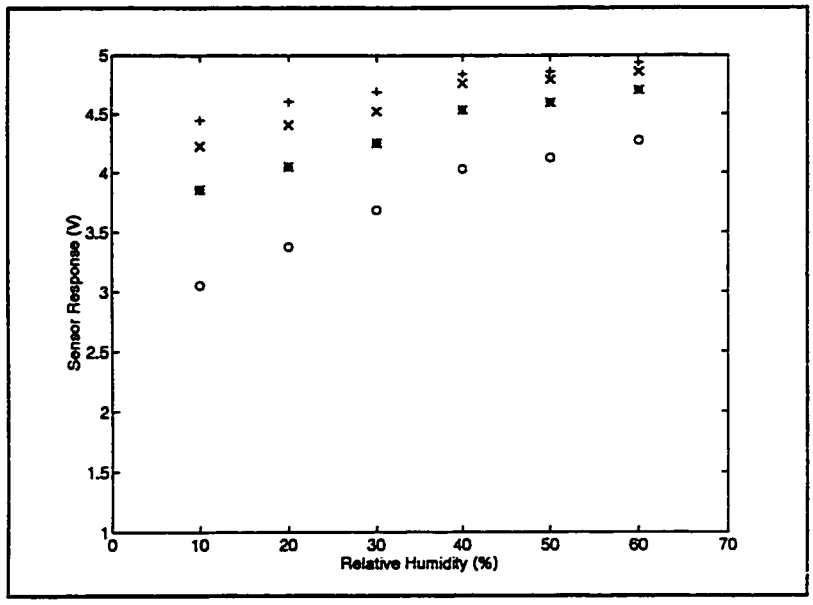

Figure 5.12: Sensor #4 (TGS813) response as a function of relative humidity at different values of propane concentration; (o) 68.5 ppm, (*) 176 ppm, (x) 336 ppm and (+) 557 ppm.

Moreover, the saturation limit was noticed to be at higher values of relative humidity for the lower values of gas concentration. This makes sense considering the mechanism of this kind of sensor by which the active part of the sensor has to share the interaction between the water molecules and the gas molecules.

As shown in the Figures (5.9-5.12), sensors #1 and #3 have almost a similar behavior with more humidity effects on sensor #3 at lower values

of propane concentration. Also, sensors #2 and #4 have almost a similar behavior. This will make it difficult to use the output of one arbitrary humidity sensor in order to make a correction or to compensate for its effect in a system of sensors, *i.e.* an array of sensors. Therefore, the best method to compensate for humidity effects in an electronic nose system seems to be using the look-up tables. This method can be described by the following steps:

- Measure the array response for a certain gas at a specific value of relative humidity, for example 20%.
- Redo the experiment for different values of relative humidity, for example at 10, 30, 40, 50, and 60%.
- Do similar experiments for the other gases under test.
- The output of each experiment (at a certain value of relative humidity) could be written in a table. This table will be used to train the NNP for the system behavior (at that certain value of relative humidity), to generate a unique pattern.

In fact, the results of the previous experiments of changing relative humidity will form our look-up tables for the neural network training procedure.

5.3 Neural Network Results

As mentioned above, the look-up tables method will be used to correct for relative humidity effects on the sensor array. A typical four tables of four experiments, conducted using methane, propane,ethylene and ethane gases (50-600ppm) at the value of 20% relative humidity and room temperature, are shown in Tables (3-6) (pages 104-107). We have generated a complete set of look-up tables for the four gases used in the system and different values of relative humidity in the range of 10% to 60% (*i.e.* 24 tables).

In each look-up table, the first 4 elemental-set patterns represent the sensors output at a certain value of gas concentration. The next four numbers (either 0.1 or 0.9) determine the output pattern corresponding to a specific gas by referring to that gas by the number 0.9 while the other are referred by 0.1. Therefore, in the training process, each gas is specified by a unique pattern given in the following way: methane gas pattern is recognized by this pattern (0.9 0.1 0.1 0.1), propane pattern is (0.1 0.9 0.1 0.1), ethylene pattern is (0.1 0.1 0.9 0.1) and ethane pattern (0.1 0.1 0.1 0.9). So, whenever the value of 0.9 appears in the output of the NNP, it should identify a certain gas depending on its position. If it appears in the first column, it indicates that the injected gas is methane. If it appears in the fourth column, it indicates that the gas is ethane, and so on. The neural network program (NNP) and

it parameters are specified in more detail elsewhere [32].

Some neural network software requires that the input training data to be normalized, *i.e.* between 0 and 1, however, this is not always the case. For example, in our case the NNP was tested many times using normalized output data and non-normalized. It was found that using the non-normalized data enhanced the output results from the neural network software since the normalized data were very close to each other increasing the difficulty in distinguishing between gases. Therefore, all the input training data sets, as shown in Tables (3-6), were non-normalized.

A resulting trained system of the NNP with the specific parameters used in its training can be seen in Table (7). As shown in there, the system appears to be learned very well as trained using the data listed in Tables (3-6) for the value of 20% relative humidity, since the first 14 data sets have the value 0.9 in the first position. This means that this target pattern is for methane, the second is for propane, the third for ethylene and the fourth is for ethane.

5.3.1 Individual Gas Results

The results of our experiments, that have been conducted by injecting one kind of gas, shows that the electronic nose system is able to discriminate and detect the kind of gas injected at any value of relative humidity within the range of 10% to 60% and for any value of gas concentration between the

range of 50ppm to 600ppm. Table (8) shows a typical output result of the system, after the training and learning procedures, for ethane gas injection at the value of 20% relative humidity and room temperature. As shown in that table, the last number, the fourth, in each four output data set is almost **0.9,** which was assigned to ethane gas in the training and learning procedure. The other three numbers, each having the value **0.1**, indicates that the gas concentration of the other three gases is zero. Therefore, the system appears to be able to detect the gas injected into the chamber. The same results were observed by doing many experiments using the other gases, *i.e.* methane, ethane and propane.

5.3.2 Gas Mixture Results

Fig.(5.13) shows the output results of the neural network program for a gas mixture of propane and ethylene measurements at 40% RH and room temperature. As indicated in Fig.(5.13), as the propane gas response (o) is increasing, the ethylene gas response (*) is decreasing. At the value of about 135 ppm for the propane concentration, a cross-over took place between the ethylene and the propane responses. This point is almost the same, 130 ppm, as the ethylene concentration in the chamber. Moreover, at the cross-over point, the neural network output shows the value of **0.5,** which could be thought as a measure of the percent concentration of each gas inside the

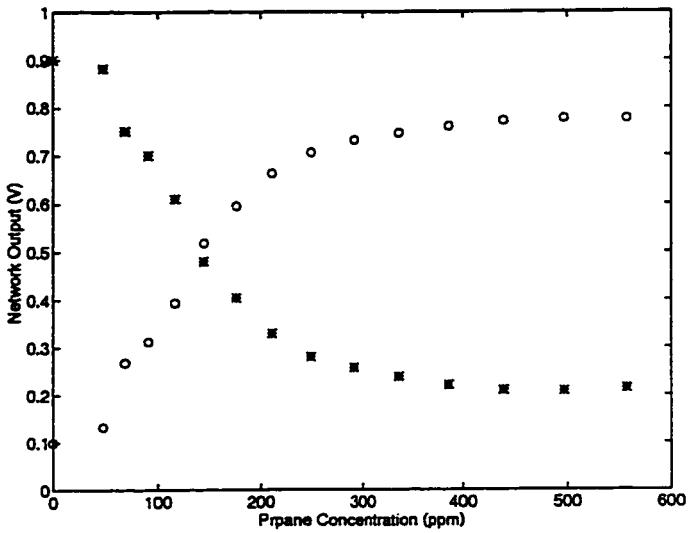

Figure 5.13: Neural network program output results for propane and ethylene gas mixture. Ethylene gas concentration (*) was constant at 130 ppm, while propane gas (o) concentration was changing in the range of 0-600 ppm. Measurements were made at room temperature and 40% relative humidity.

chamber at any point, *i.e.* the concentration of propane is 50% as well as the concentration of ethylene. For the values of concentration higher than that of the cross-over point, the propane response (neural output) continues to increase up to the value of about **0.8** and the ethylene response continues to decrease down to the value of about **0.2**. The neural network program appears to discriminate between the ethylene gas and the propane gas. Moreover, it seems to be a good tool to indicate the concentration of each one in the chamber.

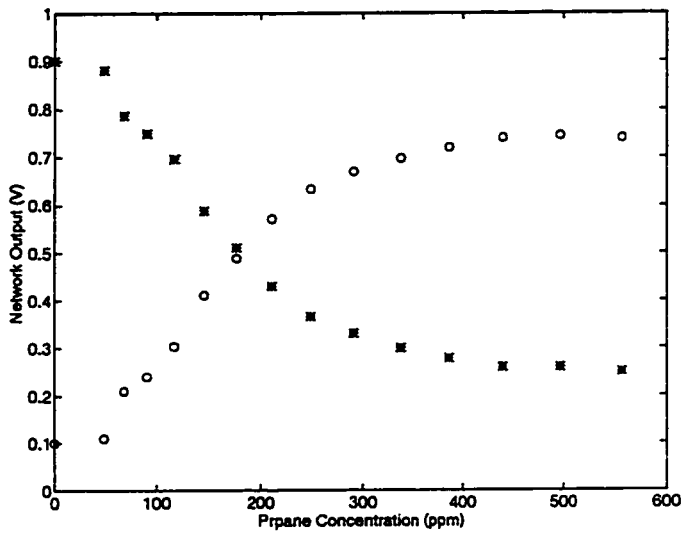

Figure 5.14: Neural network program output results for propane and ethane gas mixture. Ethane gas concentration (*) was constant at 130 ppm, while propane gas (o) concentration was changing in the range of 0-600 ppm. Measurements were made at room temperature and 40% relative humidity.

Fig.(5.14) shows the results of another experiment conducted at room temperature and the value of 40% RH for propane and ethane gas mixture. As in the propane-ethylene mixture, as the propane gas concentration increases, the neural network program output of this gas (o) is increasing. At the same time the ethane gas output response (*) started to decrease. At the point of about 170 ppm of the propane gas concentration and 0.5 of the network output, a cross-over took place. Then, the behavior continue in the same manner as before, *i.e.* increasing for the propane gas and decreasing for

the ethane gas. It appears that, as shown in Fig.(5.14), the electronic nose system is able to discriminate between two different gases mixed together in a chamber. However, its output of 0.5 now corresponds to approximately 170 ppm rather than as set by the flowmeter.

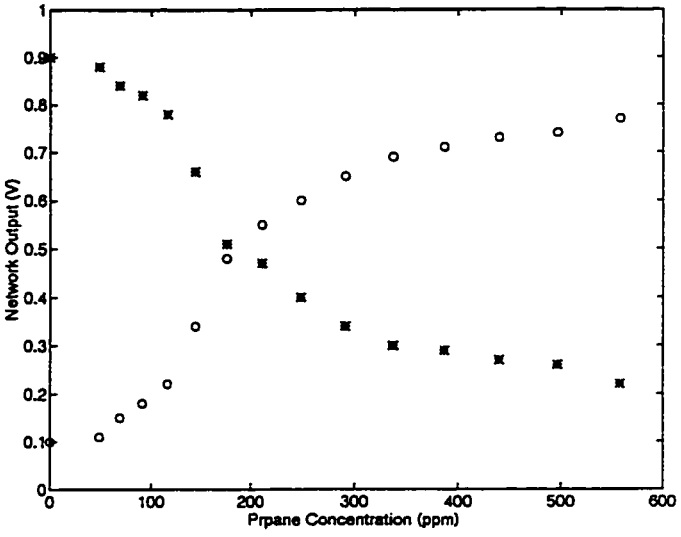

Figure 5.15: Neural network program output results for propane and ethane gas mixture. Ethane gas concentration (*) was constant at 275 ppm, while propane gas (o) concentration was changing in the range of 0-600 ppm. Measurements were made at room temperature and 50% relative humidity.

Furthermore, Fig.(5.15) shows the feasibility of the electronic nose system to discriminate between gases. Now, the value of 0.5 yields $\sim$ 180 ppm, far from the 275 ppm set by the flowmeter.. So, the problem of determining the concentration of each gas in the mixture seems to be non-trivial.

Table (3): Concordia's electronic nose results (output) for methane gas at 20% relative humidity with their pattern representation.

[C = Gas concentration (ppm), S1 = Sensor #1, S2 = Sensor #2, S3 = Sensor #3, and S4 = Sensor #4]

C	S1	S2	S3	S4				
⇓	⇓	⇓	⇓	⇓				
048.20	0.957	1.010	0.630	1.710	0.9	0.1	0.1	0.1
068.42	1.036	1.214	0.675	1.855	0.9	0.1	0.1	0.1
091.01	1.110	1.322	0.714	1.918	0.9	0.1	0.1	0.1
116.32	1.198	1.444	0.759	2.053	0.9	0.1	0.1	0.1
144.56	1.260	1.530	0.789	2.135	0.9	0.1	0.1	0.1
176.00	1.345	1.643	0.840	2.276	0.9	0.1	0.1	0.1
210.78	1.411	1.730	0.875	2.363	0.9	0.1	0.1	0.1
249.08	1.475	1.818	0.906	2.452	0.9	0.1	0.1	0.1
291.02	1.529	1.882	0.941	2.529	0.9	0.1	0.1	0.1
336.70	1.579	1.951	0.979	2.593	0.9	0.1	0.1	0.1
386.17	1.626	2.002	1.002	2.642	0.9	0.1	0.1	0.1
439.45	1.654	2.051	1.033	2.680	0.9	0.1	0.1	0.1
496.52	1.687	2.090	1.053	2.694	0.9	0.1	0.1	0.1
557.36	1.713	2.115	1.062	2.724	0.9	0.1	0.1	0.1

Table (4): Concordia's electronic nose results (output) for propane gas at 20% relative humidity with their pattern representation.

[C = Gas concentration (ppm), S1 = Sensor #1, S2 = Sensor #2, S3 = Sensor #3, and S4 = Sensor #4]

C	S1	S2	S3	S4				
⇓	⇓	⇓	⇓	⇓				
048.20	1.364	1.748	1.640	1.970	0.1	0.9	0.1	0.1
068.42	1.452	1.909	1.770	2.114	0.1	0.9	0.1	0.1
091.01	1.557	2.053	1.901	2.251	0.1	0.9	0.1	0.1
116.33	1.661	2.213	2.049	2.403	0.1	0.9	0.1	0.1
144.56	1.715	2.298	2.107	2.489	0.1	0.9	0.1	0.1
176.00	1.745	2.373	2.157	2.569	0.1	0.9	0.1	0.1
210.78	1.830	2.435	2.208	2.680	0.1	0.9	0.1	0.1
249.08	1.910	2.505	2.255	2.691	0.1	0.9	0.1	0.1
291.02	1.951	2.549	2.298	2.749	0.1	0.9	0.1	0.1
336.70	1.978	2.585	2.329	2.799	0.1	0.9	0.1	0.1
386.17	2.021	2.629	2.362	2.841	0.1	0.9	0.1	0.1
439.45	2.042	2.659	2.392	2.874	0.1	0.9	0.1	0.1
496.52	2.049	2.691	2.409	2.913	0.1	0.9	0.1	0.1
557.36	2.057	2.703	2.41	0 2.943	0.1	0.9	0.1	0.1

Table (5): Concordia's electronic nose results (output) for ethylene gas at 20% relative humidity with their pattern representation.

[C = Gas concentration (ppm), S1 = Sensor #1, S2 = Sensor #2, S3 = Sensor #3, and S4 = Sensor #4]

C	S1	S2	S3	S4				
⇓	⇓	⇓	⇓	⇓				
048.20	2.632	1.940	2.796	1.895	0.1	0.1	0.9	0.1
068.42	2.767	2.189	2.935	2.107	0.1	0.1	0.9	0.1
091.01	2.860	2.371	3.021	2.279	0.1	0.1	0.9	0.1
116.33	2.941	2.531	3.098	2.449	0.1	0.1	0.9	0.1
144.56	2.983	2.628	3.138	2.564	0.1	0.1	0.9	0.1
176.00	3.039	2.720	3.188	2.677	0.1	0.1	0.9	0.1
210.78	3.060	2.779	3.208	2.752	0.1	0.1	0.9	0.1
249.08	3.108	2.862	3.243	2.850	0.1	0.1	0.9	0.1
291.02	3.134	2.906	3.258	2.921	0.1	0.1	0.9	0.1
336.70	3.157	2.928	3.282	2.961	0.1	0.1	0.9	0.1
386.17	3.176	2.967	3.299	2.987	0.1	0.1	0.9	0.1
439.45	3.184	2.981	3.313	3.022	0.1	0.1	0.9	0.1
496.52	3.201	3.005	3.325	3.055	0.1	0.1	0.9	0.1
557.36	3.215	3.017	3.322	3.077	0.1	0.1	0.9	0.1

Table (6): Concordia's electronic nose results (output) for ethane gas at 20% relative humidity with their pattern representation.

[C = Gas concentration (ppm), S1 = Sensor #1, S2 = Sensor #2, S3 = Sensor #3, and S4 = Sensor #4]

C	S1	S2	S3	S4				
⇓	⇓	⇓	⇓	⇓				
048.20	1.350	1.471	1.373	1.709	0.1	0.1	0.1	0.9
068.42	1.447	1.687	1.483	1.889	0.1	0.1	0.1	0.9
091.01	1.494	1.881	1.560	2.066	0.1	0.1	0.1	0.9
116.33	1.573	2.077	1.651	2.245	0.1	0.1	0.1	0.9
144.56	1.650	2.218	1.720	2.370	0.1	0.1	0.1	0.9
176.00	1.730	2.350	1.807	2.505	0.1	0.1	0.1	0.9
210.78	1.805	2.450	1.870	2.610	0.1	0.1	0.1	0.9
249.08	1.864	2.561	1.931	2.718	0.1	0.1	0.1	0.9
291.01	1.895	2.618	1.967	2.775	0.1	0.1	0.1	0.9
336.70	1.928	2.665	1.993	2.824	0.1	0.1	0.1	0.9
386.17	1.982	2.712	2.038	2.878	0.1	0.1	0.1	0.9
439.45	2.021	2.759	2.079	2.925	0.1	0.1	0.1	0.9
496.52	2.046	2.793	2.098	2.959	0.1	0.1	0.1	0.9
557.36	2.06 0	2.809	2.105	2.986	0.1	0.1	0.1	0.9

Table (7): The resulting trained system created by the neural network program FILE_V.DAT.

The first few numbers indicate: 56 ≡ Total number of input samples, 4 ≡ Features in input pattern, 4 ≡ output units, 1.2 ≡ Momentum rate eta, 0.6 ≡ Learning rate alpha, 1 ≡ number of hidden layers, 80000 ≡ Number of iterations, 3 ≡ Number of layers of neurodes and 0.008871 ≡ the max. error.

56 4 4 1.20 0.60 1 80000

4 3 4

8000 0.008871

0.900417	0.000001	0.00	0.099622	
0.900416	0.000001	0.00	0.099623	Methane gas
0.900411	0.000001	0.00	0.099627	
0.900407	0.000001	0.00	0.099632	
0.900401	0.000001	0.00	0.099638	
0.900391	0.000001	0.00	0.099648	
0.900372	0.000001	0.00	0.099667	
0.900347	0.000001	0.00	0.099693	
0.900310	0.000001	0.00	0.099731	
0.900204	0.000001	0.00	0.099838	
0.900102	0.000001	0.00	0.099941	*Continue* ⟹

0.899813	0.000001	0.00	0.100233	
0.899286	0.000001	0.00	0.100766	
0.899196	0.000001	0.00	0.100856	
0.099912	0.896854	0.00	0.103083	
0.099994	0.899783	0.00	0.100219	Propane gas
0.100011	0.900122	0.00	0.099889	
0.100019	0.900181	0.00	0.099834	
0.100023	0.900184	0.00	0.099833	
0.100024	0.900186	0.00	0.099831	
0.100025	0.900183	0.00	0.099834	
0.100025	0.900182	0.00	0.099835	
0.100025	0.900184	0.00	0.099834	
0.100025	0.900185	0.00	0.099833	
0.100025	0.900185	0.00	0.099833	
0.100025	0.900186	0.00	0.099831	
0.100025	0.900186	0.00	0.099831	
0.100025	0.900185	0.00	0.099832	
0.000006	0.099921	0.900295	0.10016	
0.000006	0.099921	0.900295	0.10016	
0.000006	0.099921	0.900295	0.10016	*Continue* $\Longrightarrow$

0.000006	0.099921	0.900295	0.10016	
0.000006	0.099921	0.900295	0.10016	Ethylene gas
0.000006	0.099921	0.900294	0.10016	
0.000006	0.099922	0.900290	0.10016	
0.000006	0.099929	0.900262	0.10016	
0.000006	0.099955	0.900159	0.10016	
0.000006	0.099970	0.900101	0.10016	
0.000006	0.100000	0.899981	0.10016	
0.000007	0.100052	0.899772	0.10016	
0.000007	0.100150	0.899383	0.10016	
0.000007	0.100310	0.898741	0.10016	

0.098630	0.096809	0.00	0.899076	
0.100067	0.101081	0.00	0.898716	Ethane gas
0.100091	0.101492	0.00	0.898633	
0.100070	0.100861	0.00	0.899347	
0.100066	0.099225	0.00	0.900996	
0.100064	0.100698	0.00	0.899529	
0.100064	0.099589	0.00	0.900638	
0.100064	0.099475	0.00	0.900752	
0.100064	0.100194	0.00	0.900340	*Continue* $\Longrightarrow$

0.100064	0.099275	0.00	0.900951
0.100064	0.099682	0.00	0.900545
0.100064	0.101365	0.00	0.898864
0.100064	0.100455	0.00	0.899773
0.100064	0.099144	0.00	0.901082

Table (8): The output results of the neural network program as ethane gas was injected in the range of 50-600 ppm at the value of 20% relative humidity and room temperature.

sample 0 output 0 = 0.100703

sample 0 output 1 = 0.000008

sample 0 output 2 = 0.000014

sample 0 output 3 = 0.999987

sample 1 output 0 = 0.102262

sample 1 output 1 = 0.154690

sample 1 output 2 = 0.058946

sample 1 output 3 = 0.949760

sample 2 output 0 = 0.100561

sample 2 output 1 = 0.000003

sample 2 output 2 = 0.000006

sample 2 output 3 = 0.999994

sample 3 output 0 = 0.102262

sample 3 output 1 = 0.154690

sample 3 output 2 = 0.058946

sample 3 output 3 = 0.949760

sample 4 output 0 = 0.100476

sample 4 output 1 = 0.000001

sample 4 output 2 = 0.000003

sample 4 output 3 = 0.999997

sample 5 output 0 = 0.102262

sample 5 output 1 = 0.154690

sample 5 output 2 = 0.058946

sample 5 output 3 = 0.949760

sample 6 output 0 = 0.100471

sample 6 output 1 = 0.000001

sample 6 output 2 = 0.000002

sample 6 output 3 = 0.999998

sample 7 output 0 = 0.102262

sample 7 output 1 = 0.154690

sample 7 output 2 = 0.058946

sample 7 output 3 = 0.949760

sample 8 output 0 = 0.100413

sample 8 output 1 = 0.000000

sample 8 output 2 = 0.000001

sample 8 output 3 = 0.999999

sample 9 output 0 = 0.102262

sample 9 output 1 = 0.154690

sample 9 output 2 = 0.058946

sample 9 output 3 = 0.949760

sample 10 output 0 = 0.100332

sample 10 output 1 = 0.000000

sample 10 output 2 = 0.000001

sample 10 output 3 = 0.999999

sample 11 output 0 = 0.102262

sample 11 output 1 = 0.154690

sample 11 output 2 = 0.058946

sample 11 output 3 = 0.949760

sample 12 output 0 = 0.100283

sample 12 output 1 = 0.000000

sample 12 output 2 = 0.000001

sample 12 output 3 = 0.999999

sample 13 output 0 = 0.102262

sample 13 output 1 = 0.154690

sample 13 output 2 = 0.058946

sample 13 output 3 = 0.949760

sample 14 output 0 = 0.100205

sample 14 output 1 = 0.000000

sample 14 output 2 = 0.000000

sample 14 output 3 = 1.000000

sample 15 output 0 = 0.102262

sample 15 output 1 = 0.154690

sample 15 output 2 = 0.058946

sample 15 output 3 = 0.949760

sample 10 output 0 = 0.100332

sample 10 output 1 = 0.000000

sample 10 output 2 = 0.000001

sample 10 output 3 = 0.999999

sample 11 output 0 = 0.102262

sample 11 output 1 = 0.154690

sample 11 output 2 = 0.058946

sample 11 output 3 = 0.949760

sample 12 output 0 = 0.100283

sample 12 output 1 = 0.000000

sample 12 output 2 = 0.000001

sample 12 output 3 = 0.999999

sample 13 output 0 = 0.102262

sample 13 output 1 = 0.154690

sample 13 output 2 = 0.058946

Chapter 6

Conclusions and Further Recommendations

6.1 Humidity Sensor

- A *SAW* humidity sensor based on changes in the viscoelastic properties of a thin film in addition to the mass-loading effect has been studied. The experiments carried out show a linear behavior of the sensor response in the range $0\% - 10\%$ due to the mass-loading effect, and a superposition of mass loading and viscoelastic response for higher values of $\%RH$.

- When a film was cast directly over the substrate, a turn-around in the frequency shift response and a jump in the attenuation occurred. However, when a thin metal film was deposited between the polymer and the substrate, both the turn-around and the jump were eliminated

with a remarkable decrease in the attenuation. These two observations could be explained as a result of the changes in the viscoelastic properties of the thin film (*i.e.* the plasticization effect). At the plasticization point the film changes its behavior from acoustically thin (elastic) to acoustically thick (rubbery); *i.e.* the film became lossy.

- The film thickness was found to be an important parameter to determine the turn-around value. Our results show that the thicker the film the lower the value of relative humidity at which the turn-around took place. A similar results were obtained for the jump in the insertion loss change.

- It appears that the mass-loading effect dominates for low values of relative humidity values ($0 - 10\%$), while the viscoelastic effects dominate for higher values of relative humidity ($10 - 100\%$), (in the case of a metallized path). However, when the film was cast directly over the substrate the sensor could not function at high values of relative humidity ($> 86\%$), which might be explained to be due to the high attenuation from the acoustoelectric effect.

- The sensor showed a reversible and a reproducible response with a moderate hysteresis effect of the order of 5% over the period the experiments took place.

- Due to these effects (particularly reversibility and reproducibility), the interactions between the polymer and water molecules are primarily electrostatic. There was chemisorption in the sensing process.

- Finally, the sensor has been tested with other gases and appears to be insensitive to any of them (except alcohol which dissolve the polymer), and very sensitive to humidity (*i.e.* it is selective to humidity in "free-alcohol" surroundings).

- Final conclusion: a *SAW* device consisting of polyXIO polymer film deposited on a metallized $LiNbO_3$ substrate appears to be an excellent candidate as a humidity sensor in an alcohol-free environment.

6.2 The Electronic Nose System

- An electronic nose system of four Taguchi gas sensors (TGS) was built and used to detect and discriminate between combustible gases. The results of the conducted experiments show that each sensor has a unique response pattern for each gas used in the test, and that the polyXIO *SAW* device when fully calibrated could serve as a hygrometer to select appropriate tables.

- It appears that relative humidity affects the behavior of the electronic nose system.

- The look-up tables method shows a promising approach to correct for the relative humidity effects. This was by accumulating training data at a specific relative humidity and then using these results to train the neural network program to detect each gas. Therefore, the trained system first determines the relative humidity and then looks up the appropriate set of tables for training purposes.

- The feasibility of discriminating between gases in a gas mixture analyte has been demonstrated using the look-up tables. The results show that it is feasible to discriminate between two gases; however, it appears that it not easy to predict or estimate the gas concentration in the analyte.

- The reason of the difficulties in this system was explained to be due to the operational mechanism of the TGS sensors used in the system. This means that each sensor in the system depends on the ambient conditions especially relative humidity, temperature, and the concentration of oxygen gas inside the chamber, which are varying in time. This gives a non-reproducible output from the sensors, which makes it difficult for the neural network program to be trained, for general use.

- Another approach was introduced to correct for humidity effects. This was to use one sensor to measure the humidity effects and then sub-

tract this effect from the response of each sensor. However, the results show that relative humidity affect each sensor in the array in slightly different way. This makes it impossible to cancel the humidity effect by subtracting the effect using one specific sensor.

6.3 Recommendations for Future Work

- Due to the absence of the cross effects in the SAW humidity sensor, the device could be a good sensor candidate for humidity measurements in general and to eliminate humidity effects in a specific electronic nose system.

- The effect of temperature on the SAW humidity sensor could be studied in more detail, in order to achieve a good reliable humidity sensor for a wide range of temperature.

- The SAW humidity sensor could be calibrated and used as a part of a SAW sensor array in an electronic nose system to correct for humidity effects.

- An electronic nose system based on another kind of sensors, which is less affected by ambient conditions would enhance the reproducibility of the system. This might enhance the possibility of discriminating between gases and estimating the gas concentration of each component

of a gas mixture. A SAW sensor array is proposed for this kind of study.

Bibliography

[1] N. Kinjo, S. O'Hara, T. Sugawara and S. Tsuchitani. "Changes in the Electrical Resistance of Ionic Co-Polymers Caused by Moisture Sorption and Desorption". *Polymer Journal,* **Vol. 15** *(1983), pp. 621-623.*

[2] M. Hijikigava, S.Miyoshi, T. Sugihara, and A. Jinda. "A Thin-Film Resistance Humidity Sensor". *Sensors and Actuators,* **Vol. 4,** *(1986), pp. 307-315.*

[3] Y. Sadaoka, Y. Sakai and H. Akiyama. "A Humidity Sensor Using Alkali Salt Poly(Ethylene Oxide) Hybrid Films". *Journal of material Science,* **Vol. 21,** *(1986), pp. 235-240.*

[4] Y. Sakai, Y. Sadaoka and H. Fukumoto. "Humidity-Sensitive and Water-Resistive Polymeric Materials". *Sensors and Actuators,* **Vol. 13** *(1988), pp. 243-250.*

[5] Y. Sakai, Y. Sadaoka and K. Ikeuchi. "Humidity Sensors Composed of Grafted Copolymers". *Sensors and Actuators,* **9** *(1986). pp. 125-131.*

[6] Noboru Yamazoe, Yasuhiro Shimizu. "Humidity Sensors: Principles and Applications". *Sensors and Actuators,* **10** *(1986) 379-398.*

[7] A. Venema, E. Nieuwkoop and M. J. Vellekoop, M. S. Nieuwenhuizen, A. W. Barendsz. "Design Aspects of SAW Sensors". *Sensors and Actuators,* **10**, *(1986) pp. 47-63.*

[8] Hank Wohltjen, "Mechanism of Operation and Design Considerations for Surface Acoustic Wave Device Vapour Sensors". *Sensors and Actuators,* **5** *(1984) 307-325.*

[9] Richard M. White, Peter J. Wicher, Stuart W. Wenzel and Edward T. Zellars. "Plate-Mode Ultrasonic Oscillator Sensors". *IEEE Transactions on Ultrasonics, Ferroelectric, and Frequency Control,* **Vol. UFFC-34**, *No. 2, March 1987, pp. 162-170.*

[10] S. W. Wenzel, B. A. Martin and R. M. White. "Generalized Lamb-Wave multisensor". *1988 Ultrasonics Symposium, pp. 563-567.*

[11] David S. Ballantine, Hank Wohltjen. "Surface Acoustic Wave Devices for Chemical Analysis". *Analytical Chemistry,* **Vol. 61**, *No. 11, June 1989, pp. 704A-714A.*

[12] N. Rezgui and J. F. Alder. "An RF Oscillator for 158MHz Surface Acoustic Wave Sensors (SAWS)". *Analytical Proceedings, February 1989,* **Vol. 26**, *pp46-48.*

[13] Jay W. Grate, Stephen J. Martin and Richard M. White. "Acoustic Wave Microsensors, Part1". *Analytical Chemistry,* **Vol. 65**, *No. 21, November 1,1993, pp. 940A-948A.*

[14] Jay W. Grate, Michael H. Abraham. "Review Paper: Solubility Interactions and the Design of Chemically Selective Sorbent Coatings for Chemical Sensors and Arrays". *Sensors and Actuators B,* **3** *(1991) 85-111.*

[15] T. Nomura, K. Oofuchi, T. Yasuda and S. Furukawa. "SAW Humidity sensor using Dielectric Hygroscopic Polymer Film". *Ultrasonics Symposium 1994, pp. 503-506.*

[16] Tooru Nomura, Ken Oobuchi, Tsutmu Yasuda and Shoji Furukawa. "Humidity Sensor Using Surface Acoustic Wave Delay Line with Hygroscopic Dielectric Film". *Jpn. J. Appl. Phys. Vol.* **32** *(1993) pp. 4205-4208. Part 1, No. 9B, September 1993.*

[17] Antonio J. Ricco and Stephen J. Martin. "Thin Metal Film Characterization and Chemical Sensors: Monitoring Electronic Conductivity,

Mass Loading and Mechanical Properties with Surface Acoustic Wave Devices". *Thin Solid Films,* **206** *(1991) 94-101.*

[18] Henry Wohltjen, Raymond Dessy. "Surface Acoustic Wave Probe for Chemical Analysis. I. Introduction and Instrument Description". Anal. Chem., **Vol. 51**, NO. 9, (1979) 1458-1464.

[19] Maarten S. Nieuwenhuizen, Arnold J. Nederlof and Anton W. Barendsz. "Metallophthalocyanines as Chemical Interfaces on a Surface Acoustic Wave Gas Sensor for Nitrogen Dioxide". *Anal. Chem., 1988,* **60**, *230-235.*

[20] Antonio J. Ricco. "SAW Chemical Sensors: An Expanding Role with global impact". *The Electrochemical Society Interface (Winter 1994), pp.38-44.*

[21] Stephen J. Martin, George C. Frye and Stephen D. Senturla. "Dynamics and Response of Polymer-Coated Surface Acoustic Wave Devices: Effect of Viscoelastic Properties and Film Resonance". *Anal. Chem. 1994,* **66**, *2201-2219.*

[22] Manabu Sato, Tastuo Yamamoto Masao Takeuchi and Kazuhiko Yamanouchi. "Humidity Sensitivity of Lamb Waves on Composite

Polymide/ZnO/Si_3N_4 Structure". *Jpn. J. Appl. Phys., Vol. 32 (1993) pp. 2380-2383.*

[23] R. M. White and F. W. Voltmer. "Direct Piezoelectric Coupling to Surface Elastic Waves". *Appl. Phys. Lett.*, **7** *(1965)314-316.*

[24] Martin Viens, J. David N. Cheeke. "Highly Sensitive Temperature Sensor Using SAW Resonator Oscillator". *Sensors and Actuators A*, **24** *(1990) 209-211.*

[25] D. E. Cullen and G. K. Montress. "Progress in the development of SAW Resonator Pressure Transducers". *1980 Ultrasonic Symposium, 1980 IEEE, pp. 696-701.*

[26] Persaud and G. H. Dodd, "Analysis of Discrimination Mechanisms in the Mammalian Olfactory System Using a Model Nose". *Nature (London),* **299** *(1982) 352-355.*

[27] S. Zarcomb and J. R. Stretter. "Theoretical Basis for Identification and Measurement of Air Contaminants Using an Array of Sensors Having Partially Overlapping Sensitivity". *Sensors and Actuators,* **6** *(1984) 225-243.*

[28] B. H. Jennings. "The Thermal Environment, Conditioning and Control". *Harper & Row, Publishers, 1978, Ch. 3.*

[29] Roger Colby Legg. "Air Conditioning Systems, Design, Comissioning and Maintenance". *B. T. Bastford Ltd, London, 1991, Ch. 1.*

[30] Edward G. Pita. "Air Conditioning Principles and Systems, an Energy Approach". *Printice Hall, Englewood Cliffs, New Jersey 07632, 1989, 2nd Edition, Ch. 16.*

[31] M. F. Lawrence, Z. Huang, C. H. Langford and I. Ordonez. "Photocurrent Generation and Charge Transport in SnO2 /Ion Exchange Polymer-ZnTPP/Au Cells". *J. Phys. Chem. 1993,* **97**, *944-951.*

[32] Allan M. Sitar. "The Environmental Electronic Nose". *M.Sc Thesis, Concordia University 1995.*

[33] U. Weimar, K. D. Schierbaum and W. Gopel. "Pattern Recognition Methods for Gas Mixture Analysis: Application to Sensor Arrays Based upon SnO_2". *Sensors and Actuators,* **B1** *(1990) 93-96.*

[34] P. Romppainen, V. Lantto and S. Leppavuori. "Effect of Water Vapour on the response Behavior of Tin Dioxide Sensors in Constant Temperature-pulsed Modes of Operation". *Sensors and Actuators,* **B1** *(1990) 73-78.*

[35] Paul E. Keller, Lars J. Kangas, Lars H. Liden, Sherif Hashem and Richard T. Kouzes. "Electronic Noses and Their Applications". *IEEE Northcon/Technical Applications Conference (TAC'95)*

[36] H. V. Shurmer, J. W. Gardner and P. Corcoran. "Intelligent Vapour Discrimination Using a Complete 12-Element Sensor Array". *Sensors and Actuators,* **B1** *(1990) 256-260.*

[37] David S. Ballantine, Jr., Susan L. Rose and Jay W. Grate, Hank Wohltjen. "Correlation of Surface Acoustic Wave Device Coating Responses with Solubility Properties and Chemical Structure Using Pattern Recognition". *Anal Chem., 1986,* **58**, *3058-3066.*

[38] Susan L. Rose-Pehrsson and Jay Grate, David S. Ballantine, Jr., Peter C. Jurs. "Detection of Hazardous Vapors Including Mixtures Using Pattern Recognition Analysis of Responses from Surface Acoustic Wave Devices". *Anal. Chem., 1988,* **60**, *2801-2811.*

[39] Edward T. Zellers, Samuel J. Patrash, and Guo-Zheng Zhang. "Selective Measurements of Organic Vapors Using SAW Sensors with Reactive or Sorptive Coatings: Steric, Electronic, and Solubility Factors". *1991 IEEE, pp.998-1001.*

[40] Jun Li. "A Mixed Gas Sensor System Based on Thin Film SAW Sensor Array and Neural Network". *1993 IEEE, pp. 170-181.*

[41] J. Reichert, W. Coerdt and H. J. Ache. "Development of a Surface Acoustic Wave Sensor Array for the Detection of Methanol in Fuel Vapours". *Sensors and Actuators B,* **13-14**, *(1993) 293-296.*

[42] Edward T. Zellers, Tin-Su Pan, Samuel J. Patrash, Mingwei Han and Stuart A. Batterman. "Extended Disjoint Principal-Components Regression Analysis of SAW Vapor Sensor-Array Responses.

[43] B. A. Auld. "Acoustic Fields and Waves in Solids". *Wiley, New York, 1973.*

[44] G. S. Kino. "Acoustic Waves: Devices, Imaging, and Analog Signal Processing". *Prince-Hall, Inc., New Jersey, 1986.*

[45] Falconer, Robert S. "A Theoretical and Experimental Study of a Conductivity-Based Surface Acoustic Wave Gas Microsensor". *Maine University, Ph. D. Dissertation, 1993.*

[46] A. J. Ricco, S. J. Martin and T. E. Zipperian. "Surface Acoustic Wave Gas Sensor Based on Film Conductivity Changes". *Sensors and Actuators,* **8** *(1985) 319-333.*

[47] Jay Grate, Stephen J. Martin and Richard White. "Acoustic Wave Microsensors, Report, Part II". *Anal. Chem.* **Vol. 65**, *No. 22, November 15,1993.*

[48] Jay Grate and Mark Klusty, R. Andrew McGill, Michael H. Abraham, Gray Whiting and Jenik Andonian-Haftvan. "The predominant role of swelling-induced modules changes of the sorbent phase in determining the responses of polymer-coated surface acoustic wave vapor sensors". *Anal. Chem. 1992,* **64**, *610-624.*

[49] S. J. Martin and G. C. Frye. "Surface Acoustic Wave Response to Changes in Viscoelastic Film Properties". Appl. Phys. Lett. 57 (18), 29 October 1990.

[50] Zdravko P. Khlebarov, Any I. Stoyanova and Diana I. Topalova. "Surface Acoustic Wave Gas Sensors". *Sensors and Actuators B,* **8**, *(1992) 33-40.*

[51] R. Lec, J. F. Vetelino, R. S. Falconer and Z. Xu. "Macroscopic Theory of Surface Acoustic Wave Gas Microsensors". *1988 Ultrasonics symposium, pp.585-589.*

[52] J. D. Galipeau, R. S. Falconer, J. F. Vetelino, J. C. Andle, E. L. Wittman and M. G. Schweyer. "Theory, design and operation of a surface acoustic Wave Hydrogen Sulfide Microsensor". *Laboratory for Science and Tech-*

nology and Department of Electrical and Computer Engineering, University of Maine, Orono, ME 04469 and Andreson Laboratories Inc., Bloomfield, CT 06002.

[53] Ferry, J. D. "Viscoelastic Properties of Polymers". *3rd ed.; Wiley: New York, 1980, Ch1 & Ch2.*

[54] S. J. Martin, A. J. Ricco, and G. C. Frye. "Utilization of Polymer Viscoelastic Properties in Acoustic Wave Sensor Applications". *Appl. Phys. Lett.* **57** *(18), 29 October 1990, pp.1867-1869.*

[55] G. M. Magomedov, Z. R. Radahabov, G. P. Mashinskaya and A. B. Aizavov. "Anisotropy of the Viscoelastic Properties of Laminated Organometallic Plastics". *Mechanics of Composite Materials,* **Vol. 25**, *Iss: 5, pp. 559-63 (1989).*

[56] J. W. Gardner, E. L. Hines and M. Wilkinson. "Application of Artificial Neural Networks to an Electronic Olfactory System". *Meas. Sci. Technol.* 1 *(1990) 446-451.*

[57] T. Nakamoto and T. Moriizumi. "Oder Sensor Using Quartz-Resonator Array and Neural-Network Pattern Recognition". *1988 Ultrasonics Symposium, pp. 613-616.*

[58] "Electronic Noses". *Analytical Chemistry*, **Vol 63**, *No. 10, May 15, 1991. pp. 585A-588A.*

[59] Andreas Mandelis and Constantinos Christofides. "Physics, Chemistry and Technology of Solid State Gas Sensor Devices". *Wiley &Son, Inc. Ch6-ch7.*

[60] Benoit L'Archevque. Development and Characterization of a Polymer-Based Impedance Variation Hygrometer. Concordia University, Internal Report for CHEM 450, Chemistry Department, 1992.

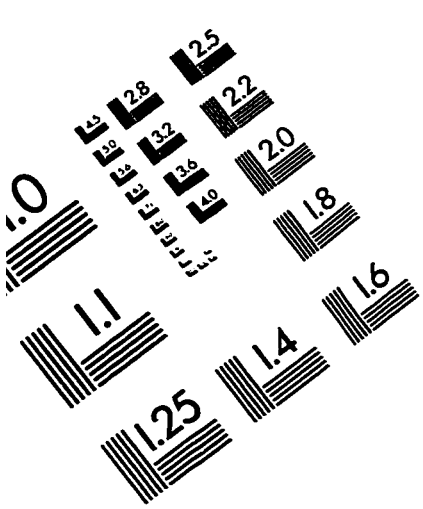

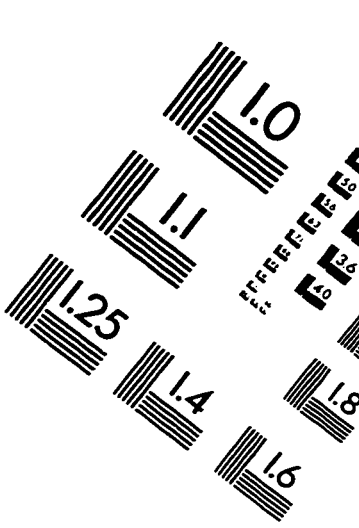

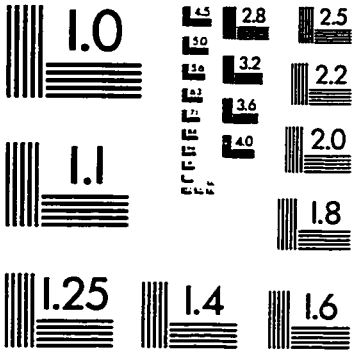

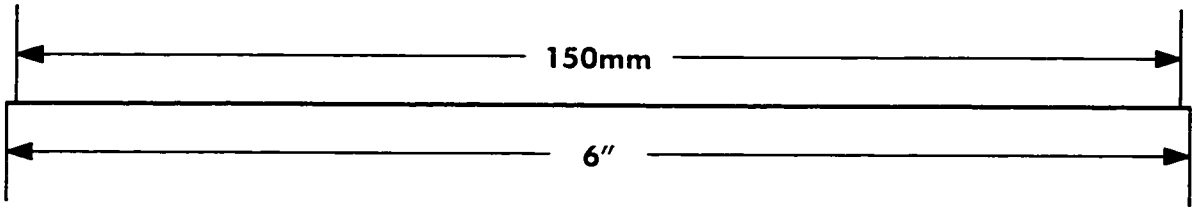

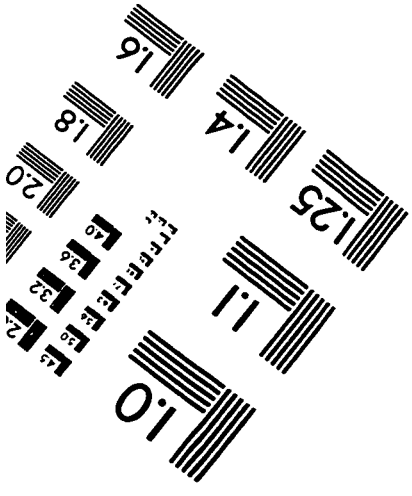

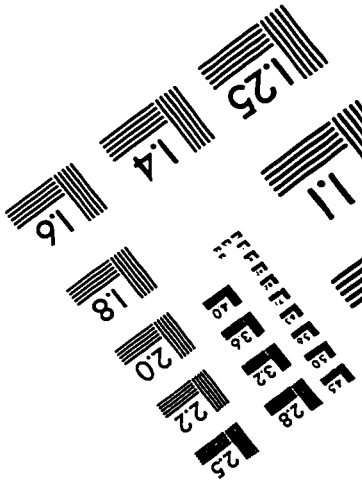

APPLIED IMAGE, Inc
1653 East Main Street
Rochester, NY 14609 USA
Phone: 716/482-0300
Fax: 716/288-5989